Research Square

Preprints are preliminary reports that have not undergone peer review.
They should not be considered conclusive, used to inform clinical practice,
or referenced by the media as validated information.

PRMT1 mediated methylation of YBX1 promotes tumorigenicity of glioblastoma stem cells

Ji Wang

wangji0720@yeah.net

University of Science and Technology of China https://orcid.org/0000-0002-2657-9132

Shiquan Shen

Dongshan Zhang

Zongyu Xiao

Tianran Chai

Nan Peng

Xuanzhi Wang

Jingpeng Guo

Honglong Zhou

Liang Chen

Minghui Zeng

Long Zhang

Yang Tu

Li Jia

Shengyuan Ni

Zheng Li

Qing LAN

Second Affiliated Hospital of Soochow University Department of Neurosurgery https://orcid.org/0000-0002-8468-4942

Haibo Wu

the First Affiliated Hospital of USTC, Division of Life Sciences and Medicine, University of Science and Technology of China https://orcid.org/0000-0003-0817-9191

Lin Wang

Fei Wang

Article

Keywords:

Posted Date: July 16th, 2026

DOI: https://doi.org/10.21203/rs.3.rs-10282905/v1

License: This work is licensed under a Creative Commons Attribution 4.0 International License.
Read Full License

Additional Declarations: There is **NO** conflict of interest to disclose.

PRMT1 mediated methylation of YBX1 promotes tumorigenicity of glioblastoma stem cells

Ji Wang[1], Shiquan Shen[2], Dongshan Zhang[3], Zongyu Xiao[4], Tianran Chai[3], Nan Peng[1], Xuanzhi Wang[1], Jingpeng Guo[5], Honglong Zhou[6], Liang Chen[7], Minghui Zeng[1], Long Zhang[1], Yang Tu[1], Li Jia[1], Shengyuan Ni[1], Zheng Li[1], Qing Lan[2], Haibo Wu[8], Lin Wang[1], Fei Wang[1]

[1]Department of Neurosurgery, The First Affiliated Hospital of USTC, Division of Life Sciences and Medicine, University of Science and Technology of China, Hefei, Anhui, 230001, China.

[2]Department of Neurosurgery, The Second Affiliated Hospital of Soochow University, Suzhou, Jiangsu, 215000, China.

[3]Department of Neurosurgery, Institute of Neuroscience, The Second Affiliated Hospital of Guangzhou Medical University, Guangzhou, 510260, China.

[4]Department of Neurosurgery, The Fourth Affiliated Hospital of Soochow University, Suzhou, Jiangsu, 215123, China.

[5]Department of Neurosurgery, Fu Yang People's Hospital, Fuyang, Anhui, 236001, China.

[6]Department of Neurosurgery, The Second Affiliated Hospital of Nanchang University, Nanchang, Jiangxi, 330006, China.

[7]Department of Pathology, PanYu Hospital GuangZhou University of Chinese Medicine, Guangzhou, 511400, China.

[8]Department of Pathology and Intelligent Pathology Institute, The First Affiliated Hospital of USTC, Division of Life Sciences and Medicine, University of Science and Technology of China, Hefei, Anhui, 230001, China.

Corresponding authors: Ji Wang, wangji0720@yeah.net; Qing Lan, szlq006@163.com; Haibo Wu, wuhaibo@ustc.edu.cn; Lin Wang, wl-doctor@163.com; Fei Wang, neurosurgeonwf1@ustc.edu.cn.

These authors contributed equally: Ji Wang, Shiquan Shen, Dongshan Zhang, Zongyu Xiao.

ABSTRACT

Glioblastoma (GBM) is the most lethal primary malignant tumor of the adult central nervous system, with glioblastoma stem cells (GSCs) driving tumor progression, treatment resistance, and relapse. Protein arginine methyltransferase 1 (PRMT1) is aberrantly dysregulated in various cancers and is associated with poor prognosis in glioma; However, the critical substrates and molecular mechanisms underlying GSC malignancy remain largely unclear. This study identifies the multifunctional RNA-binding protein Y-box binding protein 1 (YBX1) as a direct substrate of PRMT1. PRMT1 mediates the asymmetric dimethylation of YBX1 at arginine 69 (R69) within its cold-shock domain. Functional experiments, both *in vitro* and *in vivo*, confirm that PRMT1 knockdown or chemical inhibition significantly represses GSC proliferation, self-renewal, and tumorigenesis, while overexpression of enzymatically active PRMT1-unlike its catalytically inactive mutant-restores malignant characteristics. Mechanistically, PRMT1 activates the AKT signaling cascade, leading to YBX1 Ser102 phosphorylation and subsequent nuclear import. Furthermore, PRMT1-catalyzed dimethylation of YBX1 at R69 enhances its binding to m5C-modified mRNAs of core cell cycle genes PKMYT1 and CDCA5, stabilizing these transcripts and accelerating GSC cell cycle progression. Consistently, a methylation-deficient YBX1-R69K mutant fails to rescue the proliferative and self-renewal deficits resulting from endogenous YBX1 deletion. A cell-penetrating peptide targeting the YBX1 R69 methylation motif effectively inhibits YBX1 methylation and induces significant anti-tumor effects in GBM xenografts. Clinically, the levels of YBX1-R69 asymmetric dimethylation are positively correlated with PRMT1 abundance, higher tumor grades, and reduced overall survival in patient glioma tissues. In summary, this study reveals an unreported oncogenic PRMT1-YBX1 signaling cascade that sustains GSC malignant features through arginine post-translational modification and mRNA stabilization. Targeting PRMT1-dependent YBX1 arginine methylation may represent a promising therapeutic strategy against GBM.

INTRODUCTION

Glioblastoma (GBM), classified by the WHO as a grade 4 diffuse glioma, represent the

most aggressive and lethal primary malignant tumor of the adult central nervous system [1]. Although multimodal treatment, which includes maximal surgical resection, radiotherapy, and chemotherapy, has led to some improvement in disease management, the survival benefit for patients remains limited [2]. In recent years, significant efforts have been dedicated to both optimizing standard therapeutic regimens and developing innovative treatment strategies, such as immunotherapy and oncolytic virotherapy [3-5]. Recent advancements in molecular pathology have refined our understanding and classification of glioma, highlighting that this disease is characterized not only by rapid progression, diffuse infiltration, and frequent recurrence, but also by significant heterogeneity [6, 7]. Glioblastoma stem cells (GSCs) are increasingly recognized as a key cellular component contributing to this heterogeneity [8]. Beyond their numerical prevalence, GSCs represent the core cell population that drives malignant progression in GBM. Incomparison to bulk tumor cells, GSCs demonstrate significantly enhanced self-renewal capabilities, multilineage differentiation potential, and strong tumor-initiating abilities, which allow them to continuously replenish the tumor cell pool and sustain intratumoral heterogeneity [9]. In parallel, GSCs are centrally implicated in therapeutic resistance. They evade conventional radio chemotherapy by upregulating DNA damage repair mechanisms, maintaining a quiescent state, enhancing anti-apoptotic pathways, and adapting to hypoxic and perivascular niches [10, 11]. These therapy-resistant GSCs can subsequently repopulate the tumor, acting as the cellular ‘seeds’ of recurrence [9]. Beyond facilitating recurrence, GSCs actively modify the vascular niche, sustain a hypoxic microenvironment, and promote an immunosuppressive tumor milieu, thereby driving invasion, pathological angiogenesis, and immune evasion [9, 10, 12]. Collectively, these attributes underscore that the significance of GSCs lies not in their abundance, but in their unique ability to determine whether a GBM can sustain growth, withstand therapy, relapse, and evolve into a more invasive and immunologically privileged state. Consequently, GSCs serve as a central node for deciphering the mechanisms underlying GBM genesis, progression, and recurrence, while also representing a crucial entry point for the development of novel targeted agents, the optimization chemoradiotherapy combinations, and the design of

effective immunotherapeutic strategies. Given this pivotal role, elucidating the molecular mechanisms that maintain GSC stemness and proliferative fitness is of paramount importance for developing more effective interventions. Although recent studies have identified various signaling, epigenetic, and post-transcriptional regulatory networks involved in GBM progression [13, 14], the precise molecular dependencies that sustain GSC-driven malignant behavior remain incompletely understood.

Among the regulatory mechanisms contributing to the maintenance of GSCs, post-translational modifications (PTMs) have garnered significant attention. PTMs modify protein function without altering the genomic sequence, and their dysregulation is frequently observed in cancer [15]. A diverse array of PTM types, including ubiquitination, deubiquitylation, phosphorylation, and methylation, as well as recently identified modifications such as lactylation, succinylation, and SUMOylation, along with their various substrates, forms a complex regulatory network that profoundly influences GSC behavior [16]. In the context of methylation, two primary categories have been studied in GSCs: classic histone methylation, which regulates stemness and differentiation, and non-histone methylation, with particular emphasis on protein arginine methylation [14, 17]. Catalyzed by the protein arginine methyltransferase (PRMT) family, this modification regulates cellular behavior through the methylation of both histone and non-histone substrates. While histone arginine methylation contributes to epigenetic regulation of gene expression, methylation of non-histone proteins can influence their stability, activity, interactions, and subcellular localization [18]. Among the members of the PRMT family, PRMT1 is the predominant type I enzyme found in mammalian cells, responsible for the majority of asymmetric dimethylarginine (aDMA) modifications. Increasing evidence has linked dysregulation of PRMT1 expression or activity to several hallmarks of cancer, including malignant progression, metabolic rewiring, immune evasion, and therapeutic resistance [19]. In glioma, elevated PRMT1 expression has been correlated with poor clinical outcome and malignant progression [20]. However, the downstream substrates and molecular mechanisms through which PRMT1 supports the maintenance of GSC maintenance and tumor propagation remain inadequately defined.

Y-box binding protein 1 (YBX1) is a multifunctional nucleic acid-binding protein belonging to the cold-shock protein family. It regulates various aspects of gene expression, including transcription, mRNA stability and translation [21]. As a reader of 5-methylcytosine (m5C)-modified transcripts, YBX1 plays a crucial role in post-transcriptional gene regulation by influencing the stability and fate of target mRNAs [22]. Aberrant expression of YBX1 has been documented in numerous human malignancies, where it correlates with tumor progression, therapeutic resistance, and poor clinical outcome. In addition to its general role in cancer, YBX1 regulates cancer stem cells in various tumor types, including lung cancer, leukemia, and hepatocellular carcinoma, through distinct mechanisms such as modulation of the Wnt pathway or m6A RNA methylation [23-25]. In GSCs, YBX1 is phosphorylated by PLK1, which facilitates its translocation to the nucleus. Once in the nucleus, phosphorylated YBX1 activates the expression of stemness marker genes, enhances the repair of DNA damage induced by temozolomide and inhibits apoptosis [26]. Additionally, YBX1 in teracts with long non-coding RNAs such as DARS1-AS1, which leads to the stabilization of stemness-associated mRNAs including FOXM1 [27]. Collectively, these findings position YBX1 as a central hub that sustains the viability, stemness, and therapeutic resistance of GSCs. These observations indicate that the oncogenic activity of YBX1 is regulated not only at the expression level, but also through post-translational modifications that influence its functional state. Beyond phosphorylation, YBX1 undergoes O-linked N-acetylglucosamine (O-GlcNAc) modification at threonine 57 (T57), which stabilizes the protein and increases its expression. This modification also promotes YBX1 phosphorylation at serine 102, facilitating its nuclear translocation and enhancing the transcription of glycolysis-related genes, thereby stimulating lactate production [28]. Furthermore, PRMT5-mediated methylation of YBX1 at R205 has been shown to regulate NF-κB activity in colorectal cancer [29]. However, it remains completely unknown whether YBX1 is directly regulated by PRMT1-mediated arginine methylation, whether this modification is necessary for its tumorigenic activity in GSCs, and how this event affects downstream RNA regulatory programs.

Here, we identify YBX1 as a direct substrate of PRMT1 and demonstrate that

PRMT1 catalyzes the methylation of YBX1 at Arg69 within its cold-shock domain. Functionally, this site-specific modification is essential for GSC self-renewal and GBM progression. Mechanistically, PRMT1 promotes AKT activation, and phosphorylation of AKT at Ser473 enhances YBX1 phosphorylation at Ser102, thereby facilitating its nuclear translocation. Additionally, PRMT1 associates with YBX1 and mediates asymmetric dimethylation at Arg69, a modification that enhances YBX1 binding to *PKMYT1* and *CDCA5* mRNAs, consequently increasing the stability of these transcripts. Importantly, targeting YBX1 methylation suppresses GSC proliferation, self-renewal, and tumorigenicity. Together, these findings establish PRMT1-dependent YBX1 methylation as a critical driver of GBM progression and highlight the PRMT1-YBX1 axis as a potential therapeutic vulnerability.

RESULTS

PRMT1 is enriched in tumor cell populations and correlates with poor prognosis in glioma

To characterize the cellular distribution of PRMT1 in solid tumors, we integrated several recently published single-cell RNA-sequencing datasets. PRMT1 was predominantly expressed in malignant cells, exhibiting significantly higher expression levels compared to immune cells, monocytes/macrophages, oligodendrocytes, astrocytes, and endothelial cells (Fig. 1A-F). Notably, PRMT1 expression remained elevated across various malignant states, including AC-like, OC-like, OPC-like, and NPC-like populations. These findings suggest that PRMT1 is closely associated with the malignant cellular compartment and may contribute to tumor cell-intrinsic progression. We subsequently examined the clinical relevance of PRMT1 in glioma. Analysis of the CGGA database revealed that PRMT1 expression was significantly higher in high-grade gliomas compared to low-grade gliomas, and it was also elevated in IDH wild-type gliomas, a molecular subtype linked to poorer prognosis (Fig. 1G, H). Kaplan-Meier analysis further revealed that elevated PRMT1 expression is associated with poorer survival outcomes in both the overall glioma cohort and in the IDH wild-type subgroup (Fig. 1I, J). Similar results were observed in the TCGA database, where PRMT1 expression was found to be increased in high-grade and IDH wild-type gliomas,

correlating with unfavorable prognosis (Fig. 1K-N). To validate these findings in patient samples, we conducted immunohistochemical staining on 44 glioma tissues of varying grades, alongside non-tumor brain tissues. The results demonstrated that PRMT1 expression was significantly higher in glioma tissues compared to non-tumor controls, with an even greater increase noted in grade 3-4 gliomas relative to grade 2 gliomas (Fig. 1O). Consistently, quantitative analysis indicated a significantly higher proportion of PRMT1-high cases in high-grade gliomas, whereas the majority of non-tumor tissues displayed low PRMT1 expression (Fig. 1P). Collectively, these findings indicate that PRMT1 is aberrantly upregulated in glioma cells and is linked to malignant progression and poor clinical outcomes.

PRMT1 promotes GSC proliferation and self-renewal

To investigate the functional contribution of PRMT1 to glioblastoma progression, we examined its effects on the proliferation and self-renewal of GSCs. Initially, we assessed the expression levels of PRMT1 across a panel of GSCs using western blotting. Based on the observed variations in endogenous PRMT1 expression, we selected GSC23, GSC11, and GSC464 for further experimentation (Fig. S1A). Subsequently, we established stable PRMT1 knockdown models in the PRMT1-high GSC23 and GSC11 cells, while generating overexpression models of either PRMT1-WT or the catalytically inactive PRMT1-G80R in the PRMT1-low GSC464 cells. RT-qPCR and western blotting analyses confirmed effective PRMT1 depletion and ectopic expression in these models. Importantly, the levels of H4R3me2a, a canonical histone methylation mark mediated by PRMT1, varied in accordance with PRMT1 expression; however, the PRMT1-G80R mutant did not affect H4R3me2a levels (Fig. 2A, B). Additionally, pharmacological inhibition of PRMT1 using AMI-1 also resulted in a reduction of H4R3me2a abundance (Fig. S1B), indicating that PRMT1's function in GSCs is reliant on its methyltransferase activity. We then evaluated whether PRMT1 regulates GSC proliferation. CCK-8 assays demonstrated that PRMT1 knockdown significantly inhibited the proliferation of GSC23 and GSC11 cells, whereas ectopic expression of PRMT1-WT in GSC464 cells markedly promoted cell growth. In contrast, overexpression of the catalytically inactive PRMT1-G80R mutant had a minimal

impact (Fig. 2C, D). Consistent results were obtained from EdU assays, which demonstrated that the depletion of PRMT1 reduced the proliferative capacity of GSC11 or GSC23 cells. In contrast, PRMT1-WT, but not PRMT1-G80R, was found to promote DNA synthesis in GSC464 cells (Fig. 2I, J; Fig. S1F, G). These findings indicate that PRMT1 enhances GSC proliferation in an activity-dependent manner. Given that self-renewal is a defining characteristic of GSCs and a critical factor in the propagation of glioblastoma, we further investigated the impact of PRMT1 on stem-like growth. Extreme limiting dilution analysis (ELDA) revealed that PRMT1 knockdown significantly impaired the self-renewal capacity of GSC23 and GSC11 cells, whereas overexpression of PRMT1-WT enhanced self-renewal in GSC464 cells. Notably, the PRMT1-G80R mutant did not exhibit a comparable effect (Fig. 2E, F; Fig. S1E). Consistent with these observations, neurosphere formation assays demonstrated that PRMT1 depletion markedly reduced sphere size, while PRMT1-WT overexpression resulted in increased neurosphere growth; this effect was absent in the G80R mutant (Fig. 2G, H; Fig. S1C, D). Together, these results support the role of PRMT1 in maintaining GSC self-renewal and stem-like growth. Given the robust pro-proliferative effects of PRMT1 observed *in vitro*, we next evaluated its role in tumor growth *in vivo* using an orthotopic xenograft model. Equal numbers of control and PRMT1-depleted GSC23 cells were intracranially implanted into nude mice, and followed by monitoring of animal survival (Fig. 2M). The knockdown of PRMT1 significantly extended the overall survival of tumor-bearing mice. Histologic analysis further indicated that tumors derived from PRMT1-depleted cells were markedly smaller compared to those in the control group, as assessed by H&E staining (Fig. 2K). Moreover, immunohistochemical staining revealed a reduction in Ki67 expression in PRMT1-deficient tumors (Fig. 2K). Quantitative analysis of tumor sections confirmed that PRMT1 depletion significantly reduced tumor burden and proliferative activity *in vivo* (Fig. 2L, N). Collectively, these *in vitro* and *in vivo* data illustrate that PRMT1 drives GSC proliferation, self-renewal, and tumor growth in a manner dependent on its methyltransferase activity.

PRMT1 interacts with YBX1 and regulates its phosphorylation in GSCs

To further elucidate the mechanism by which PRMT1 promotes the proliferation and self-renewal of GSCs, we performed liquid chromatography-tandem mass spectrometry (LC-MS/MS) on GSC23, GSC11, and HEK293T cells overexpressing PRMT1. Venn diagram analysis revealed 21 candidate PRMT1-interacting proteins that were common across these cellular contexts (Fig. 3A). Among these, YBX1 attracted our attention due to its established role as an oncogenic regulator in glioma [27, 30]. Consequently, we hypothesized that PRMT1 may facilitate glioblastoma progression through its interaction with YBX1. To investigate whether PRMT1 physically interacts with YBX1, we first assessed their subcellular localization by immunofluorescence. Our results indicated that PRMT1 was predominantly localized in the nucleus, while YBX1 was present in both the nucleus and cytoplasm, suggesting a potential nuclear interaction between the two proteins (Fig. 3B). We subsequently conducted endogenous co-immunoprecipitation (Co-IP) assays in GSC23 and GSC11 cells. Using an anti-PRMT1 antibody for Co-IP, we detected the YBX1 protein signal within the co-precipitated complex. Conversely, reciprocal immunoprecipitation with an anti-YBX1 antibody similarly revealed the presence of PRMT1 (Fig. 3C). To further corroborate this interaction, we ectopically expressed PRMT1-FLAG and YBX1-HA in HEK293T cells and performed exogenous Co-IP assays, which confirmed the association between PRMT1 and YBX1 (Fig. 3D). Collectively, these findings demonstrate that PRMT1 physically associates with YBX1. We then investigated whether PRMT1 regulates YBX1 expression. RNA-seq and proteomic analyses indicated that modulation of PRMT1 did not affect YBX1 mRNA or total protein levels (Fig. 3E, F), a result further validated by RT-qPCR and western blotting analyses in PRMT1 knockdown and overexpression models (Fig. 3G, H). Similar findings were observed following pharmacologic inhibition of PRMT1 with AMI-1, which also did not alter total YBX1 expression (Fig. S2A, B). Conversely, modulation of YBX1 did not impact PRMT1 expression (Fig. S2C-F). These findings suggest that PRMT1 and YBX1 do not mutually regulate each other at the transcriptional and translational levels. However, western blot analysis revealed that either the reduction of PRMT1 expression or its pharmacological inhibition significantly decreased the phosphorylation level of YBX1

at the Ser102 site (Fig. 3H). Given that Ser102 phosphorylation is essential for the oncogenic activity of YBX1 [31], it is hypothesized that PRMT1 may enhance GSC proliferation and self-renewal by modulating the phosphorylation of YBX1 rather than its expression.

PRMT1 regulates YBX1 phosphorylation and nuclear translocation through AKT activation in GSCs

Since PRMT1 is a protein arginine methyltransferase that does not directly mediate the phosphorylation process, we hypothesized that its influence on YBX1 phosphorylation might be indirect. Previous studies have reported that AKT phosphorylates YBX1 and promotes its activation [31, 32], prompting us to investigate whether PRMT1 regulates the AKT-YBX1 axis. Immunoblotting analysis showed that PRMT1 knockdown significantly reduced AKT phosphorylation at Ser473 without affecting the total AKT protein levels in GSCs (Fig. 4A). Similar results were observed following pharmacological inhibition of PRMT1 with AMI-1 (Fig. 4B), whereas ectopic expression of PRMT1 led to increase p-AKT (Ser473) levels without altering the total AKT abundance (Fig. 4C). These findings suggest that PRMT1 positively regulates AKT activation. To determine whether AKT mediates the PRMT1-regulated phosphorylation of YBX1, we treated the cells with the AKT inhibitor MK2206. The inhibition of AKT phosphorylation markedly decreased YBX1 phosphorylation at Ser102, yet total YBX1 protein levels remained unaffected (Fig. 4D), in line with previous reports [31, 32]. Notably, the combined depletion of PRMT1 and MK2206 treatment further reduced p-AKT (Ser473) and p-YBX1 (Ser102) levels compared to MK2206 treatment alone (Fig. 4E, F), supporting the hypothesis that PRMT1 regulates YBX1 phosphorylation through AKT activity. Finally, we investigated the interaction between AKT and YBX1. Exogenous Co-IP assays in HEK293T cells demonstrated that AKT associates with YBX1, and endogenous Co-IP further validated this interaction in GSCs (Fig. 4G, H), corroborating previous studies [31, 32]. Given that AKT-dependent phosphorylation is essential for the nuclear translocation and function of YBX1, we evaluated the impact of PRMT1 on the subcellular distribution of YBX1. Immunofluorescence analysis showed that the knockdown of PRMT1 significantly

diminished the accumulation of YBX1 in the nucleus (Fig. 4I; Fig. S3A), while the overexpression of PRMT1 enhanced YBX1's localization in the nuclear compartment in HEK293T cells (Fig. 4J). Additionally, nuclear-cytoplasmic fractionation experiments demonstrated that PRMT1 depletion resulted in a decrease in nuclear YBX1 levels and an increase in cytoplasmic YBX1 levels, without affecting the total levels of YBX1 (Fig. 4K; Fig. S3B). Conversely, PRMT1 overexpression led to the opposite outcomes (Fig. 4L). Together, these results demonstrate that PRMT1 facilitates YBX1 phosphorylation and its nuclear ltranslocation via AKT activation (Fig. 4M).

PRMT1 catalyzes asymmetric dimethylation of YBX1 at R69 in GSCs

Given that PRMT1 physically interacts with YBX1 but does not regulate its expression, we hypothesized that PRMT1 may modulate YBX1 through arginine methylation. To investigate this possibility, GSCs were treated with the PRMT1 inhibitor AMI-1 or the broad methyltransferase inhibitor AdOx, followed by endogenous Co-IP to assess levels of asymmetric dimethylarginine (aDMA). Both treatments significantly reduced aDMA signals in whole-cell lysates and immunoprecipitated fractions (Fig. S4A), indicating that PRMT1 contributes to the arginine methylation associated with YBX1 in GSCs. Consistently, exogenous Co-IP assays showed that co-expression of PRMT1 and YBX1 elevated aDMA levels compared to single transfection (Fig. S4B, C). Likewise, PRMT1 overexpression increased aDMA abundance, whereas the catalytically inactive PRMT1-G80R mutant exhibited minimal effect (Fig. S4D, E). Collectively, these data suggest that PRMT1 regulates the arginine methylation of YBX1. To further elucidate the relevant interaction and methylation site, we generated a series of HA-tagged YBX1 truncation and point mutants, including complete or partial deletions of the cold shock domain (CSD) (Fig. 5A). The AlphaFold3-based prediction identified R69 as the residue with the higher binding score (Fig. 5B). Moreover, the amino acid sequence surrounding R69 exhibited a high degree of conservation across species (Fig. S4F), underscoring its potential functional significance. Notably, the deletion of the CSD region (Δ52-129), and to a lesser extent the deletion of residues 61-70, significantly impaired the PRMT1-YBX1 interaction (Fig. 5C; Fig. S4G), indicating that the CSD region is essential for efficient binding. We then investigated whether PRMT1 regulates

the asymmetric dimethylation of YBX1 at R69. Endogenous Co-IP experiments demonstrated that PRMT1 depletion markedly reduced YBX1-R69me2a levels in immunoprecipitated fractions, accompanied by decreased aDMA signals in the corresponding lysates (Fig. 5D). Conversely, PRMT1 overexpression resulted in the opposite effect (Fig. 5E). Consistent with these findings, both selective inhibition of PRMT1 and broad suppression of PRMT activity led to a decrease in global aDMA abundance and a reduction in YBX1-R69me2a levels (Fig. 5F; Fig. S4H, I). A similar reduction in YBX1-R69me2a was observed following AdOx treatment under conditions of YBX1 overexpression (Fig. 5G). In contrast, the YBX1-R69K mutant displayed minimal basal YBX1-R69me2a signal and was largely unresponsive to methyltransferase inhibition (Fig. S4J), suggesting that R69 is the primary methylation site regulated by PRMT1. To further confirm the specificity of this modification, we re-expressed PRMT1 in PRMT1-deficient GSC models, which partially rescued both global aDMA abundance and YBX1-R69me2a levels in stable PRMT1-deficient cells (Fig. 5H; Fig. S4L). In parallel, the genetic or pharmacological inhibition of PRMT1 significantly decreased the levels of YBX1-R69me2a in cells expressing YBX1-WT, while little to no effect was observed in cells expressing the YBX1-R69K mutant, where YBX1-R69me2a remained barely detectable (Fig. 5I; Fig. S4K). Similarly, overexpression of PRMT1 enhanced the asymmetric dimethylation of YBX1-WT, but this effect was absent in the YBX1-R69K mutant (Fig. 5J). Furthermore, treatment with the methylated peptide resulted in reduced YBX1-R69me2a levels compared to the corresponding unmethylated peptide in the YBX1-WT context, whereas no such reduction was noted in the R69K mutant (Fig. 5K). Collectively, these findings demonstrate that PRMT1 specifically catalyzes the asymmetric dimethylation of YBX1 at residue R69.

PRMT1-mediated YBX1 methylation at R69 is indispensable for GSC proliferation and self-renewal

While the oncogenic role of YBX1 in glioma is well-established, the functional significance of its post-translational asymmetric dimethylation at Arginine 69 remains largely unexplored. To determine whether PRMT1-mediated methylation of YBX1 is

essential for driving the proliferation and self-renewal of GSCs, we established stable rescue models by reintroducing wild-type YBX1 (YBX1-WT) or a methylation-defective mutant (YBX1-R69K) into YBX1-knockout (YBX1-KO) GSCs (Fig. 6A). Phenotypic assays revealed that exogenous YBX1-WT fully rescued the severe proliferation defects caused by YBX1 depletion. In stark contrast, the YBX1-R69K mutant failed to restore GSC proliferation (Fig. 6B; Fig. S5A). Consistently, *in vitro* ELDA demonstrated that YBX1-KO significantly compromised the self-renewal capacity of GSC23 and GSC11 cells. This deficiency was robustly rescued by YBX1-WT, but not by the YBX1-R69K mutant (Fig. 6C; Fig. S5B, C). To evaluate the *in vivo* requirement for this specific modification, we established orthotopic xenograft mouse models and monitored survival until the humane endpoint (Fig. 6F). Histological assessment revealed that YBX1-KO essentially abolished intracranial tumor formation. Strikingly, reintroduction of YBX1-WT completely restored tumorigenicity, while the YBX1-R69K mutant achieved only marginal rescue, leading to significantly reduced tumor burdens (Fig. 6D, E). IHC profiling of xenografts confimed these observations; the drastically decreased expression of Ki67 and YBX1-R69me2a in YBX1-KO tumors was effectively restored by YBX1-WT, but only partially recovered in the YBX1-R69K group (Fig. 6D, G, H). Given the critical dependence of GSC proliferation and self-renewal on YBX1 methylation, we next explored the translational potential of targeting this modification in glioblastoma. We engineered a cell-permeable, competitive unmethylated YBX1 peptide containing the R69 consensus site, which was conjugated to a TAT sequence. A pre-methylated peptide and a vehicle treatment served as negative controls (Fig. 6I). Co-IP analyses indicated that the non-methylated peptide, rather than the methylated peptide, specifically and competitively inhibited endogenous YBX1 R69 methylation in GSCs (Fig. 6J). Importantly, neither peptide disrupted the physical interaction between PRMT1 and YBX1, confirming the specificity of the unmethylated peptide as a competitive substrate (Fig. 6K; Fig. S5D, E).

Functionally, treatment with the non-methylated peptide significantly blunted the proliferation of GSCs compared to the methylated control (Fig. 6L, M). Furthermore, ELDA results demonstrated that the non-methylated peptide profoundly impaired the

self-renewal capabilities of GSC23 and GSC11 cells, an effect that was entirely absent in the methylated peptide group (Fig. 6N; Fig. S5F). Finally, we evaluated the *in vivo* anti-tumor efficacy of this peptide using a subcutaneous xenograft model. Administration of the non-methylated peptide almost completely halted subcutaneous GBM growth, whereas the methylated control provided no therapeutic benefit (Fig. 6O, Q). This potent anti-tumor efficacy was further evidenced by a striking suppression in Ki67 positivity in the resected tumors (Fig. 6P, R). Collectively, these findings highlight the targeted blockade of YBX1 methylation as a highly promising therapeutic strategy for GBM.

The PRMT1-YBX1 axis regulates the cell cycle progression of GSCs by directly stabilizing PKMYT1 and CDCA5 transcripts

To elucidate the downstream regulatory network orchestrated by the PRMT1-YBX1 axis, we first integrated our RNA-seq data with publicly available enhanced UV crosslinking and immunoprecipitation (eCLIP)-seq datasets from U251 cells to map the direct YBX1 interactome. The intersection of these datasets yielded 7 high-confidence candidate genes that are strictly regulated by the PRMT1/YBX1 axis in GBM cells (Fig. 7A). We then further analyzed the RNA-seq datasets from PRMT1-knockdown and YBX1-knockdown GBM cells. The venn diagram intersection revealed 91 overlapping genes that were consistently downregulated under both conditions, and bioinformatics analysis highlighted a striking enrichment of these shared targets in biological processes governing cell cycle phase transition and DNA replication (Fig. S6A). Consistent with these transcriptomic alterations, flow cytometric analysis revealed that PRMT1 depletion induced a pronounced G1-phase arrest accompanied by a concomitant reduction in G2-phase cells. Conversely, ectopic overexpression of PRMT1 elicited the opposite effect, promoting G1-to-G2 cell cycle progression (Fig. S6B, C). Manipulation of YBX1 expression can replicate similar cell cycle phenotypes (Fig. S6D, E). Molecular validation through western blotting demonstrated that the levels of key cell cycle regulators, including E2F1, Cyclin D1, CDK2, CDK1, and Cyclin B1, were drastically reduced following the knockdown of PRMT1 or YBX1. Conversely, the expression of negative regulators P21 and P53 was markedly elevated (Fig. S6F, H). In

contrast, overexpression of PRMT1 or YBX1 resulted in opposite trends in the expression of these cell cycle markers (Fig. S6G, I). Guided by the notable cell cycle phenotype and our multi-omic screening, we focused in on PKMYT1 and CDCA5 as the principal downstream effectors of the PRMT1-YBX1 axis. Further analysis of the YBX1 eCLIP-seq peaks identified CAUC as the most enriched 4-nucleotide motif, which corresponds precisely to the canonical YBX1 core RNA-binding consensus (Fig. 7B). Notably, eCLIP-seq tracks demonstrated pronounced YBX1 binding peaks across the transcripts of *PKMYT1* and *CDCA5* (Fig. 7C). In addition, clinical data from the CGGA database indicated strong positive correlations between PRMT1 or YBX1 expression and the levels of PKMYT1 or CDCA5 in glioma samples (Fig. S7A-D). RT-qPCR and immunoblotting confirmed that the mRNA and protein levels of PKMYT1 and CDCA5 were positively regulated by the expression status of PRMT1 and YBX1 in GSCs (Fig. 7D-K).

To ascertain the physical interaction between YBX1 and its target transcripts, we performed RNA immunoprecipitation (RIP)-qPCR, which confirmed the robust enrichment of *PKMYT1* and *CDCA5* mRNAs by the YBX1 protein in GSCs (Fig. 7L, M). Notably, the binding affinity of YBX1 to these transcripts was significantly impaired following PRMT1 knockdown (Fig. 7N, O), whereas PRMT1 overexpression enhanced this interaction (Fig. S7E). The suggests that PRMT1-mediated methylation may facilitate the recognition and binding capacity of YBX1 to target mRNAs. To mechanistically, evaluate whether this axis governs RNA stability, we monitored mRNA decay kinetics after Actinomycin D-induced transcriptional blockade. The results demonstrated that depletion of either PRMT1 or YBX1 dramatically accelerated the degradation of *PKMYT1* and *CDCA5* transcripts (Fig. 7P-S), while their overexpression significantly prolonged mRNA half-lives (Fig. S7F-I). Collectively, these findings establish that the PRMT1-YBX1 axis promotes glioblastoma progression by enhancing the mRNA stability of critical cell cycle regulators. Since YBX1 is recognized as a canonical "reader" of m5C-modified transcripts, we hypothesized that the m5C methyltransferase NSUN2 might coordinate with the PRMT1-YBX1 axis. Although bulk tumor analysis from the CGGA dataset revealed a relatively modest

clinical correlation between NSUN2 and PKMYT1/CDCA5 (Fig. S7J, K), our *in vitro* mechanistic investigations uncovered a distinct cooperative interplay. Specifically, NSUN2 expression in GSCs robustly upregulated the transcription of *PKMYT1* and *CDCA5* (Fig. S7L-O). Furthermore, YBX1-RIP-qPCR combined with RNA decay assays elucidated that NSUN2 expression not only enhanced the recognition of *PKMYT1* and *CDCA5* mRNAs by YBX1, but also synergistically amplified their RNA stability (Fig. S7P-U). Thus, the m5C "writer" NSUN2 synergizes with the PRMT1-YBX1 complex to sustain oncogenic mRNA stabilization in GSCs.

Clinical hyperactivation of the PRMT1-YBX1 axis correlates with glioma progression and dictates poor patient survival

To establish the clinical relevance of our mechanistic findings, we evaluated the abundance of YBX1-R69me2a in human glioma specimens. IHC profiling revealed a robust upregulation of YBX1-R69me2a in high-grade gliomas (WHO grade 3 and GBM) compared to non-tumor brain tissues (Fig. 8A). Crucially, statistical analysis of this clinical cohort demonstrated a progressive enrichment of YBX1-R69me2a that closely paralleled the advancing WHO histological grades (Fig. 8B). Furthermore, quantitative assessment of these tumor specimens unveiled a significant positive correlation between endogenous YBX1-R69me2a and PRMT1 expression levels ($R = 0.407$) (Fig. 8C). Supporting these histological observations, western blotting of fresh clinical cohorts revealed a coordinated hyperactivation of this oncogenic network. Specifically, the protein levels of PRMT1, YBX1-R69me2a, PKMYT1, CDCA5, and NSUN2 were consistently elevated in glioma tissues compared to non-tumor controls (Fig. 8D). Expression correlation analyses further strengthened our *in vitro* mechanistic model, revealing robust positive correlations between PRMT1 expression and the clinical abundance of YBX1-R69me2a, PKMYT1, and CDCA5 (Fig. 8E-G). Importantly, we investigated whether aberrant activation of this signaling cascade correlates with adverse clinical outcomes. Kaplan-Meier survival analyses clearly demonstrated that glioma patients with high levels of either PRMT1 or YBX1-R69me2a experienced profoundly shorter overall survival (OS) compared to patients with low expression of these markers (Fig. 8H, I). Taken together, these clinical data

not only validate the pathological existence of the PRMT1-YBX1-PKMYT1/CDCA5 axis in human glioma, but also underscore PRMT1-mediated YBX1 methylation as a potent prognostic biomarker and a compelling therapeutic target.

DISCUSSION

In this study, we identify YBX1 as a direct substrate of PRMT1 and demonstrate that PRMT1 catalyzes the asymmetric dimethylation of YBX1 at Arg69 within its cold-shock domain. This site-specific modification is functionally essential for glioma stem cell self-renewal and the progression of GBM. Mechanistically, PRMT1 operates through two complementary pathways: it activates AKT phosphorylation, which in turn interacts with YBX1 to promote its nuclear translocation via Ser102 phosphorylation. Concurrently, within the nucleus, PRMT1 physically interacts with YBX1 and catalyzes the asymmetric dimethylation at Arg69, thereby enhancing the stability of PKMYT1 and CDCA5 transcripts and promoting their expression (Fig. 8J). Importantly, the disruption of Arg69 methylation, either through genetic ablation or competitive blockade using a non-methylated peptide, significantly suppresses GBM growth both *in vitro* and *in vivo*. These findings indicate that YBX1 methylation is not merely a correlative event but a functional determinant of tumor propagation, thereby identifying the PRMT1-YBX1 axis as a therapeutically actionable vulnerability in GBM.

PRMT1 is the predominant type I protein arginine methyltransferase in mammalian cells, playing crucial physiological roles in maintaining hematopoietic, muscle, and neural stem cell homeostasis [33-35]. Dysregulated expression or activity of PRMT1 has been linked to malignant progression, metabolic adaptation, immune evasion, and therapeutic resistance in cancer [19]. Supporting this broad oncogenic spectrum, PRMT1 has been shown to facilitate stem-like programs across multiple malignancies. In chronic myeloid leukemia stem cells, PRMT1-mediated H4R3me2a promotes *RPL29* transcription and enhances global protein synthesis [36]. In esophageal squamous cell carcinoma-initiating cells, PRMT1 activates Wnt and Notch signaling to promote self-renewal and chemoresistance [37]. In skin tumor-initiating cells, PRMT1 collaborates with PRMT5 and ULK3 to regulate chromatin remodeling and stemness-

associated programs. Additionally, in liver cancer-initiating cells PRMT1 has been implicated in controlling mitochondrial fission [38]. In glioma, elevated PRMT1 expression correlates with poor prognosis, increased proliferation, PTX3-linked ferritinophagy, and resistance to radiotherapy [20, 39]. Although recent multi-omics analyses suggest that PRMT1 may coordinate nitric oxide metabolism, GBM stem cell maintenance, and remodeling of the immune microenvironment, the mechanistic basis for these effects remains poorly defined [40, 41]. Our work demonstrates that PRMT1 is not merely elevated in GSCs, but is functionally required for their proliferative and self-renewing capacity.

To elucidate the downstream mechanisms by which PRMT1 promotes GSC proliferation and GBM progression, we performed co-immunoprecipitation followed by mass spectrometry, identifying YBX1 as a candidate PRMT1-interacting protein. We subsequently confirmed that PRMT1 and YBX1 interact within the nucleus. YBX1 is a multifunctional nucleic acid-binding protein recognized as a reader of m5C-modified transcripts, with its function closely tied to subcellular localization. It has been implicated in tumor initiation, proliferation, metastasis, and therapeutic resistance across various cancer types [42, 43]. Furthermore, YBX1 is modulated by diverse post-translational modifications, including phosphorylation, ubiquitination, acetylation, and glycosylation, all of which collectively influence its protein function, nucleocytoplasmic shuttling, RNA-binding behavior, and interaction networks [44]. The arginine methylation of YBX1 has only recently been recognized as an additional regulatory layer. Previous studies have shown that PRMT5-dependent YBX1 methylation participates in inflammatory signaling, while PRMT3-mediated methylation of other residues can regulate YBX1 phase separation in colorectal cancer [29, 45]. However, whether PRMT1 directly regulates YBX1 has not yet been established. By integrating structural prediction, mutant constructs, and rescue experiments, we reveal an unrecognized event wherein PRMT1 catalyzes the asymmetric dimethylation of YBX1 at Arg69. Given that Arg69 resides within the cold-shock domain, a region critical for nucleic acid recognition and RNA binding, this modification is likely to influence the RNA-binding behavior and functional output of

YBX1. Notably, the methylation-deficient YBX1 R69K mutant was unable to rescue the proliferative and stemness defects resulting from YBX1 loss, and a non-methylated peptide similarly inhibited tumor growth. These findings suggest that the methylation state of YBX1 represents a biologically meaningful and therapeutically exploitable target.

Previous studies have established that YBX1 interacts with factors such as *DARS1-AS1* to stabilize the transcripts of *E2F1* and *FOXM1*, thereby sustaining GSC self-renewal [27]. We integrated RNA sequencing, eCLIP, and Gene Ontology analysis to identify PKMYT1 and CDCA5, two genes involved in cell cycle progression and DNA replication, as common downstream effectors of PRMT1 and YBX1. RIP-qPCR, actinomycin D chase experiments, and functional rescue assays support a model in which PRMT1-dependent Arg69 methylation prolongs the half-lives of m5C-modified *PKMYT1* and *CDCA5* mRNAs, leading to the accumulation of their protein products and enhanced the proliferation of GSCs. Concurrently, our data suggest that NSUN2 also contributes to this regulatory axis, consistent with the emerging view that m5C-dependent transcript fate is determined by cooperative interactions among writers, readers, and associated RNA-binding factors [46]. Although we did not detect a direct physical interaction between PRMT1 and NSUN2, such cooperation may still occur at the transcript level, where NSUN2-deposited m5C marks could facilitate YBX1 recognition and PRMT1-dependent methylation may further enhance the stabilizing function of YBX1 on selected mRNAs.

The significant reliance of GSCs on the PRMT1-YBX1 axis presents a promising avenue for therapeutic intervention. Pharmacological inhibition of PRMT1 using AMI-1 effectively suppresses GSC growth, thereby validating PRMT1 as a viable drug target. However, considering the essential functions of PRMT1 in maintaining physiological homeostasis, global enzymatic inhibition may pose risks to normal stem cell populations. This clinical challenge highlights the conceptual significance of our competitive peptide strategy. By selectively disrupting the methylation state of YBX1 rather than broadly affecting the PRMT1 protein complex, this approach offers enhanced specificity and potentially fewer off-target effects. This specificity is

particularly important, as the methylation state of YBX1, rather than its overall abundance, may be the primary driver of malignancy in certain contexts. Nonetheless, both AMI-1 and the peptide strategy are preliminary proof-of-concept approaches; further research is required to optimize delivery, stability, blood-brain barrier penetration, and pharmacokinetic properties before considering therapeutic translation.

Phosphorylation of YBX1 at Ser102 is a well-established prerequisite for its nuclear translocation [47]. Our observations indicate that PRMT1 modulates levels of p-YBX1 (Ser102) by activating the upstream kinase AKT (p-Ser473), without affecting the total protein levels of AKT. Reciprocal Co-IP assays further confirmed the interaction between AKT and YBX1, while inhibition of AKT hindered YBX1's nuclear entry [48]. Despite these insights, certain limitations persist. The precise biochemical intermediates through which PRMT1 activates AKT require further investigation. Moreover, the clinical utility of the PRMT1-YBX1-R69me2a axis as a prognostic biomarker necessitates validation in larger, prospective multi-institutional cohorts. In summary, our study reveals a previously unrecognized mechanism by which PRMT1 sustains YBX1 methylation to promote GSC self-renewal and GBM progression. These findings provide a novel molecular framework for understanding malignant persistence in GBM and establish the PRMT1-YBX1 axis as a promising therapeutic target.

MATERIALS AND METHODS

Clinical specimens

This study received approval from the Ethics Committee of The First Affiliated Hospital of USTC, Division of Life Sciences and Medicine (Ethics No. USTC-AH-2024031). A total of 45 clinical specimens were collected following surgical tumor resection, which included 39 glioma samples and 6 non-neoplastic brain tissues. The glioma cohort comprised 13 low-grade cases (WHO grade 2), 13 high-grade cases (WHO grade 3), and 13 glioblastoma (GBM) cases. Written informed consent was obtained from all participants prior to the collection of specimens.

Cell lines and cell culture

Five human GSC lines (GSC267, GSC464, GSC23, GSC11, and GSC91) were provided by Dr. Ming Li from the Department of Neurosurgery at the University of

Minnesota. The GSCs were cultured in DMEM/F12 (1:1) medium (Gibco, Cat.#11320033) supplemented with B27 (Invitrogen, Cat.#A5047601), recombinant human EGF (20 ng/mL, MCE, Cat.#HY-P7071), and recombinant human bFGF (20 ng/mL, MCE, Cat.#HY-P7072). Normal Human Astrocytes (NHA) and HEK293T cells were obtained from the Cell Bank of the Chinese Academy of Sciences (Shanghai, China), were cultured in Dulbecco's Modified Eagle Medium (DMEM, Gibco, Cat.#11965092) supplemented with 10% fetal bovine serum (FBS, Gibco, Cat.#10099141C) at 37°C in a humidified atmosphere containing 5% CO_2.

Limiting dilution assay

GSC23, GSC11, or GSC464 cell spheres were dissociated into single cells using accutase (Invitrogen, Cat.#A1110501). Then, GSCs were counted and plated in 96-well plates at densities of 200, 100, 50, 20, and 10 cells per well (ten replicate wells per density) in 100 μL of GSC medium. Tumorsphere formation was evaluated after 10 days, and the frequency of GSCs was calculated by extreme limiting dilution analysis (ELDA, http://bioinf.wehi.edu.au/software/elda/).

Co-immunoprecipitation (Co-IP) assay

Endogenous Co-IP: GSC23 and GSC11 cells were homogenized in NP-40 lysis buffer (Beyotime, Cat.#P0013F). Following the collection of the total protein lysate, 10% was reserved as the input control. The remainder was pre-cleared by rotating with 30 μL of Protein A/G magnetic beads (Thermo Fisher, Cat.#88803) equilibrated in TBS for 1 h at 4°C. The pre-cleared supernatant was then incubated overnight at 4°C with rotation using anti-PRMT1 (Abcam, Cat.#ab73246), anti-YBX1 (Proteintech, Cat.#20339-1-AP), anti-AKT (Proteintech, Cat.#10176-2-AP), or control IgG antibodies (Proteintech, Cat.#30000-0-AP). Immune complexes were captured by adding TBS-equilibrated Protein A/G magnetic beads and rotating for an additional 2 h at 4°C. The precipitated proteins were subsequently analyzed by immunoblotting with anti-PRMT1, anti-YBX1, anti-AKT, anti-YBX1-R69me2a (GL Biochem Shanghai) , or anti-aDMA antibodies.

Exogenous Co-IP: For exogenous Co-IP, HEK293T cells were transfected with the specified plasmids, and lysates were prepared accordingly. Ten percent of the lysate

was reserved as input, while the remaining supernatant was incubated overnight at 4°C with rotation using anti-FLAG (Selleck, Cat.#B26101) or anti-HA (Selleck, Cat.#B26202) magnetic beads. The immunoprecipitated complexes were subsequently analyzed by immunoblotting with anti-FLAG, anti-HA, anti-YBX1-R69me2a, or anti-aDMA antibodies.

RNA stability assay

To assess mRNA stability, cells were exposed to actinomycin D (MCE, Cat.#HY17559, 5 μg/mL) for 0, 2, 4, or 8 h. Total RNA was then extracted, and the remaining levels of *CDCA5* and *PKMYT1* mRNA were quantified by RT-qPCR, with β-actin serving as the internal reference. Each time point included three technical replicates, and the full stability curve experiment was repeated three independent times.

RNA immunoprecipitation (RIP) assay

RIP assays were conducted using the Magna RIP Kit (Millipore, Cat.#17-700) in accordance with the manufacturer's protocol. In brief, cells were lysed in a buffer containing protease and RNase inhibitors (Beyotime, Cat.#ST507/Cat.#R0102). The lysates were then incubated overnight at 4°C with rotation using protein A/G magnetic beads pre-coated with anti-YBX1 antibody (Proteintech, Cat.#20339-1-AP). Following immunoprecipitation, the beads were treated with proteinase K to digest the proteins, and the captured RNA was isolated by phenol-chloroform extraction. The enrichment of the target RNAs was subsequently assessed by RT-qPCR. All primer sequences are provided in Table S2. RIP experiments were performed three independent biological times with paired IgG negative controls.

Liquid chromatography-tandem mass spectrometry (LC-MS/MS) analysis

Proteins were extracted from GSC23, GSC11, and PRMT1-overexpressing HEK293T cells using NP-40 lysis buffer supplemented with protease inhibitors. The lysates were initially pre-cleared with magnetic beads and subsequently incubated overnight at 4°C with anti-PRMT1 antibody. Immune complexes were then captured by adding magnetic beads and allowing for further incubation. The resulting bead-PRMT1 antibody-protein

complexes were sent to Hangzhou Cosmos Wisdom Biotech Co., Ltd. for LC/MS analysis.

Bioinformatics analysis

The association between PRMT1 expression levels and patient prognosis in glioma was examined, with stratification based on IDH-WT and IDH-mut status, utilizing the GlioVis portal (https://gliovis.bioinfo.cnio.es/), which integrates datasets from TCGA and CGGA. Cell population classification in glioma and the single-cell expression profile of PRMT1 across various cell clusters were analyzed using the TISCH platform (https://tisch.compbio.cn/home/). Additionally, transcriptomic changes following YBX1 knockdown in GBM cells were assessed using the GSE213046 dataset. Furthermore, eCLIP-seq data were employed to identify potential RNA molecules interacting with YBX1 in GBM cells [27].

RNA sequencing and protein 4D-label free analysis

Total RNA was isolated using a RNeasy kit (Qiagen, Cat.#74106) and total protein was extracted with SDT buffer from two independent replicates of GSC23 with PRMT1 knockdown or control, as well as GSC464 with PRMT1 overexpression or control. The RNA quantity and purity of each sample were quantified. The protein suspension was lysed, extracted, and enzymatically digested, with the resulting peptides analyzed by LC-MS/MS. Quality assessment, LC-MS/MS analysis, library construction, sequencing, and data analysis were performed by Shanghai Applied Protein Technology Co., Ltd. The significance of differentially expressed genes (DEGs) was determined based on a log2(fold change) > 1 and $P < 0.05$.

Statistical analysis

Statistical analyses were performed using GraphPad Prism version 8.0 (San Diego, California, USA). The data are presented as mean ± standard deviation (SD), derived from a minimum of three independent experiments. For two-group comparisons, a two-tailed unpaired Student's t-test was utilized, while one-way analysis of variance (ANOVA) followed by Tukey's post-hoc test was employed for multiple-group

comparisons. Survival curves were constructed using the Kaplan-Meier method and analyzed with the log-rank test. A P-value of less than 0.05 was deemed statistically significant.

AUTHOR CONTRIBUTIONS

FW, LW, HBW, QL and JW designed and supervised the study. JW, SQS, DSZ, ZYX and TRC performed the experiments. NP, XZW, JPG, HLZ, MHZ, LZ and YT collected the data and performed statistical analyses. JPG, YT, XZW, LJ, SYN and ZL provided clinical samples and statistical analyses. LC performed all pathological experiments in this study. JW, SQS and FW wrote the manuscript. FW, LW, HBW, QL and JW finally reviewed the manuscript. All authors have approved the final manuscript.

ACKNOWLEDGEMENTS

We thank Professor Ming Li (Department of Neurosurgery, University of Minnesota) for kindly providing GSCs for this study. The authors are grateful for the convenience provided by all public databases used in this study (TCGA, CGGA, GEO and TISCH2). This work was supported by grants from National Natural Science Foundation of China (82303851, Ji Wang; 52473156, Fei Wang; 82460261, Honglong Zhou), Guangdong Basic and Applied Basic Research Foundation (2022A1515111065), the China Postdoctoral Science Foundation (2023M740840), the Excellent Scientific Research and Innovation Team Projects of Anhui Educational Committee (2024AH010035), the Anhui Provincial Natural Science Foundation for Young Scholars (Category A, 2508055396), and the Program of Frontier Medicine and Advanced Technology, Hefei Comprehensive National Science Center (2025IHM01050).

COMPETING INTERESTS

The authors declare no competing interests.

REFERENCES

1. Louis DN, Perry A, Wesseling P, Brat DJ, Cree IA, Figarella-Branger D, et al. The 2021 WHO Classification of Tumors of the Central Nervous System: a summary. Neuro Oncol 2021;23:1231-1251.

2. Tang J, Karbhari N, Campian JL. Therapeutic Targets in Glioblastoma: Molecular Pathways, Emerging Strategies, and Future Directions. Cells 2025;14:494.
3. Gállego Pérez-Larraya J, Garcia-Moure M, Labiano S, Patiño-García A, Dobbs J, Gonzalez-Huarriz M, et al. Oncolytic DNX-2401 Virus for Pediatric Diffuse Intrinsic Pontine Glioma. N Engl J Med 2022;386:2471-2481.
4. Ramsoomair CK, Daftari M, Benchouia R, Estevez-Ordonez D, Aka A, Himic V, et al. Locoregional delivery of CAR T cells in high-grade gliomas: a systematic analysis of safety, efficacy, and emerging biomarkers of response. J Immunother Cancer 2026;14:e014450.
5. Xu S, Tang L, Li X, Fan F, Liu Z. Immunotherapy for glioma: Current management and future application. Cancer Lett 2020;476:1-12.
6. Nicholson JG, Fine HA. Diffuse Glioma Heterogeneity and Its Therapeutic Implications. Cancer Discov 2021;11:575-590.
7. Whitfield BT, Huse JT. Classification of adult-type diffuse gliomas: Impact of the World Health Organization 2021 update. Brain Pathol 2022;32:e13062.
8. Sloan AR, Silver DJ, Kint S, Gallo M, Lathia JD. Cancer stem cell hypothesis 2.0 in glioblastoma: Where are we now and where are we going? Neuro Oncol 2024;26:785-795.
9. He J, Yan X, Hu S. Glioma stem cells: drivers of tumor progression and recurrence. Stem Cell Res Ther 2025;16:293.
10. Tang J, Amin MA, Campian JL. Glioblastoma Stem Cells at the Nexus of Tumor Heterogeneity, Immune Evasion, and Therapeutic Resistance. Cells 2025;14:562.
11. Rachamala HR, Lourembam SD, Mukhopadhyay D, Angom RS. Targeting Glioblastoma Stem Cells: Therapeutic Strategies and Clinical Perspectives. Cancers (Basel) 2026;18:1353.
12. Fei X, Wu J, Tian H, Jiang D, Chen H, Yan K, et al. Glioma stem cells remodel immunotolerant microenvironment in GBM and are associated with therapeutic advancements. Cancer Biomark 2024;41:1-24.
13. Rachamala HR, Lourembam SD, Mukhopadhyay D, Angom RS. Targeting Glioblastoma Stem Cells: Therapeutic Strategies and Clinical Perspectives.

Cancers (Basel) 2026;18:1353.
14. Cai L, Sun X, Li R, Ping Y, Lv S, Chen J. Key methylation modifications in glioma stem cells. Biochim Biophys Acta Rev Cancer 2026;1881:189527.
15. Chen Y, Ding K, Zheng S, Gao S, Xu X, Wu H, et al. Post-translational modifications in DNA damage repair: mechanisms underlying temozolomide resistance in glioblastoma. Oncogene 2025;44:1781-1792.
16. Wu J, Liu H, Li X, Huang H, Zhu H, Wang J, et al. Dysregulation of post-translational modifications in glioma: advances in pathological mechanisms and clinical targeting strategies. J Transl Med 2026;24:150.
17. Jeong Y, Cho Y, Kim YK. Protein arginine methyltransferases in cancer: mechanisms, functions, and therapeutic opportunities. J Biomed Sci 2026;33:37.
18. Wang J, Shen S, You J, Wang Z, Li Y, Chen Y, et al. PRMT6 facilitates EZH2 protein stability by inhibiting TRAF6-mediated ubiquitination degradation to promote glioblastoma cell invasion and migration. Cell Death Dis 2024;15:524.
19. Shen S, Zhou H, Xiao Z, Zhan S, Tuo Y, Chen D, et al. PRMT1 in human neoplasm: cancer biology and potential therapeutic target. Cell Commun Signal 2024;22:102.
20. Lathoria K, Gowda P, Umdor SB, Patrick S, Suri V, Sen E. PRMT1 driven PTX3 regulates ferritinophagy in glioma. Autophagy 2023;19:1997-2014.
21. Zheng X, Zeng F, Lei Y, Li Y, Deng J, Luo G, et al. YBX1: an RNA/DNA-binding protein that affects disease progression. Front Oncol 2025;15:1635209.
22. Lv F, Jin Y, Yu S, Yang X, Xia S, Ye X, et al. Emerging roles of RNA N5-methylcytosine modification in reproductive physiology and gynecological diseases. Epigenetics 2026;21:2629068.
23. Wu X, Hu Y, Ji X, Zhao Y. YBX1 promotes the stemness and metastasis of NSCLC cells by promoting CDCA8 expression. Neoplasma 2026;73:123-132.
24. Feng M, Xie X, Han G, Zhang T, Li Y, Li Y, et al. YBX1 is required for maintaining myeloid leukemia cell survival by regulating BCL2 stability in an m6A-dependent manner. Blood 2021;138:71-85.
25. Chao HM, Huang HX, Chang PH, Tseng KC, Miyajima A, Chern E. Y-box binding protein-1 promotes hepatocellular carcinoma-initiating cell progression and

tumorigenesis via Wnt/β-catenin pathway. Oncotarget 2017;8:2604-2616.
26. Li X, Chen G, Liu B, Tao Z, Wu Y, Zhang K, et al. PLK1 inhibition promotes apoptosis and DNA damage in glioma stem cells by regulating the nuclear translocation of YBX1. Cell Death Discov 2023;9:68.
27. Zheng C, Wei Y, Zhang Q, Sun M, Wang Y, Hou J, et al. Multiomics analyses reveal *DARS1-AS1*/YBX1-controlled posttranscriptional circuits promoting glioblastoma tumorigenesis/radioresistance. Sci Adv 2023;9:eadf3984.
28. Ji Y, Xu Z, Tang L, Huang T, Mu X, Ni C, et al. O-GlcNAcylation of YBX1 drives a glycolysis-histone lactylation feedback loop in hepatocellular carcinoma. Cancer Lett 2025;631:217957.
29. Hartley AV, Wang B, Mundade R, Jiang G, Sun M, Wei H, et al. PRMT5-mediated methylation of YBX1 regulates NF-κB activity in colorectal cancer. Sci Rep 2020;10:15934.
30. Wang JZ, Zhu H, You P, Liu H, Wang WK, Fan X, et al. Upregulated YB-1 protein promotes glioblastoma growth through a YB-1/CCT4/mLST8/mTOR pathway. J Clin Invest 2022;132:e146536.
31. Hong X, Li Q, Li J, Chen K, He Q, Zhao Y, et al. CircIPO7 Promotes Nasopharyngeal Carcinoma Metastasis and Cisplatin Chemoresistance by Facilitating YBX1 Nuclear Localization. Clin Cancer Res 2022;28:4521-4535.
32. Mo D, Fang H, Niu K, Liu J, Wu M, Li S, et al. Human Helicase RECQL4 Drives Cisplatin Resistance in Gastric Cancer by Activating an AKT-YB1-MDR1 Signaling Pathway. Cancer Res 2016;76:3057-66.
33. Blanc RS, Vogel G, Li X, Yu Z, Li S, Richard S. Arginine Methylation by PRMT1 Regulates Muscle Stem Cell Fate. Mol Cell Biol 2017;37:e00457-16.
34. Lynch J, Troadec E, Fung TK, Gladysz K, Virely C, Lau PNI, et al. Hematopoietic stem cell quiescence and DNA replication dynamics maintained by the resilient β-catenin/Hoxa9/Prmt1 axis. Blood 2024;143:1586-1598.
35. Hashimoto M, Takeichi K, Murata K, Kozakai A, Yagi A, Ishikawa K, et al. Regulation of neural stem cell proliferation and survival by protein arginine methyltransferase 1. Front Neurosci 2022;16:948517.

36. Zhou M, Huang Y, Xu P, Li S, Duan C, Lin X, et al. PRMT1 Promotes the Self-renewal of Leukemia Stem Cells by Regulating Protein Synthesis. Adv Sci (Weinh) 2025;12:e2308586.
37. Zhao Y, Lu Q, Li C, Wang X, Jiang L, Huang L, et al. PRMT1 regulates the tumour-initiating properties of esophageal squamous cell carcinoma through histone H4 arginine methylation coupled with transcriptional activation. Cell Death Dis 2019;10:359.
38. Goruppi S, Clocchiatti A, Bottoni G, Di Cicco E, Ma M, Tassone B, et al. The ULK3 kinase is a determinant of keratinocyte self-renewal and tumorigenesis targeting the arginine methylome. Nat Commun 2023;14:887.
39. Li H, Qi X, He L, Yang H, Ju H. PRMT1 promotes radiotherapy resistance in glioma stem cells by inhibiting ferroptosis. Jpn J Radiol 2025;43:129-137.
40. Yuk N, Jung HJ. Inhibition of PRMT1 Suppresses the Growth of U87MG-Derived Glioblastoma Stem Cells by Blocking the STAT3 Signaling Pathway. Int J Mol Sci 2024;25:2950.
41. Xue K, Gao Y, Ma C, Tang S, Tian X, Kong Y, et al. PRMT1 regulates glioblastoma stemness and immunosuppression via nitric oxide metabolism: Multi-cohort analysis and experimental validation. Nitric Oxide 2026;162:9-24.
42. Dinh NTM, Nguyen TM, Park MK, Lee CH. Y-Box Binding Protein 1: Unraveling the Multifaceted Role in Cancer Development and Therapeutic Potential. Int J Mol Sci 2024;25:717.
43. Li C, Yuan Y, Jiang X, Wang Q. Unveiling the immunological functions of the RNA m5C reader YBX1 in cancer. Front Immunol 2025;16:1703697.
44. Prabhu L, Hartley AV, Martin M, Warsame F, Sun E, Lu T. Role of post-translational modification of the Y box binding protein 1 in human cancers. Genes Dis 2015;2:240-246.
45. Shi Y, Wan T, Liu S, Liu H, Zeng Z, Li W, et al. Dynamic Arginine Methylation of YBX1 Relay Controls Its Phase Separation and Chemoradiotherapy Resistance in Rectal Cancer. Adv Sci (Weinh) 2025;12:e02786.
46. Li C, Yuan Y, Jiang X, Wang Q. Roles and mechanisms of NSUN2-mediated RNA

m5C modification in cancer progression and immune modulation. Front Immunol 2025;16:1702436.

47. Alkrekshi A, Wang W, Rana PS, Markovic V, Sossey-Alaoui K. A comprehensive review of the functions of YB-1 in cancer stemness, metastasis and drug resistance. Cell Signal 2021;85:110073.

48. Wang R, Li F, Lin Y, Lu Z, Luo W, Xu Z, et al. piR-RCC Suppresses Renal Cell Carcinoma Progression by Facilitating YBX-1 Cytoplasm Localization. Adv Sci (Weinh) 2025;12:e14398.

Figure legends

Fig. 1 PRMT1 is enriched in tumor cell populations and correlates with poor prognosis in glioma. (**A**-**F**) Cell type-specific expression of PRMT1 in published single-cell RNA-seq datasets: GSE102130 (**A**), GSE139448 (**B**), GSE131928 (**C**), GSE141383 (**D**), GSE138794 (**E**), and GSE148842 (**F**). (**G**, **H**) PRMT1 expression in LGG (WHO grade 2), HGG (WHO grade 3), and GBM samples (**G**), as well as in IDH-mutant and IDH-WT gliomas (**H**), in the CGGA cohort. (**I**, **J**) Kaplan-Meier analysis of overall survival in all glioma patients (**I**) and in IDH-WT patients only (**J**) stratified by PRMT1 expression in the CGGA cohort. (**K**, **L**) PRMT1 expression in LGG (WHO grade 2), HGG (WHO grade 3), and GBM samples (**K**), as well as in IDH-mutant and IDH-WT gliomas (**L**), in the TCGA cohort. (**M**, **N**) Kaplan-Meier analysis of overall survival in all glioma patients (**M**) and in IDH-WT patients only (**N**) stratified by PRMT1 expression in the TCGA cohort. (**O**) Representative IHC images of PRMT1 in non-tumor brain tissues, LGG (WHO grade 2), HGG (WHO grade 3), and GBM specimens. Scale bars, 50 μm. (**P**) Quantification of PRMT1 IHC staining intensity (H-score). *P < 0.05, **P < 0.01, ***P < 0.001, ****P < 0.0001; n.s: not significant.

Fig. 2 PRMT1 promotes GSC proliferation and self-renewal. (**A**) RT-qPCR analysis validating PRMT1 knockdown efficiency using two independent shRNA sequences (shPRMT1#1 and shPRMT1#2) in GSC23 and GSC11 cells, and overexpression efficiency of PRMT1-WT and the catalytic mutant PRMT1-G80R in GSC464 cells. (**B**) Western blotting analysis of PRMT1 and H4R3me2a protein levels in GSC23 and

GSC11 cells with PRMT1 knockdown, and in GSC464 cells with PRMT1-WT, or PRMT1-G80R plasmids transfection. (**C**, **D**) CCK-8 assays showing proliferation of GSC23 and GSC11 cells following PRMT1 knockdown (**C**) and of GSC464 cells following overexpression of PRMT1-WT or PRMT1-G80R (**D**). (**E**, **F**) Extreme limiting dilution analysis (ELDA) of sphere-forming frequency in GSC23 and GSC11 cells with PRMT1 knockdown (**E**) and in GSC464 cells with PRMT1-WT, or PRMT1-G80R overexpression (**F**). (**G**, **H**) Representative images of sphere formation in GSC23 and GSC11 cells following PRMT1 knockdown (**G**) and in GSC464 cells following PRMT1-WT, or PRMT1-G80R overexpression (**H**). Scale bars, 50 μm. (**I**, **J**) EdU incorporation assays showing proliferation of GSC23 and GSC11 cells following PRMT1 knockdown (**I**) and of GSC464 cells following overexpression of PRMT1-WT or PRMT1-G80R (**J**). Scale bars, 50 μm. (**K**-**N**) Orthotopic intracranial xenograft assays using GSC23 cells expressing control shRNA (Scramble) or shPRMT1. (**K**) Representative H&E staining of whole-brain sections and Ki67 immunohistochemical staining of xenograft tumors. Scale bars, 5 mm for H&E images and 50 μm for Ki67 staining. (**L**) Quantification of tumor area in each group. (**M**) Kaplan-Meier survival curves of tumor-bearing mice; P values were determined by the log-rank test. (**N**) Quantification of Ki67 staining intensity (H-score) in xenograft tumors. *$P < 0.05$, ****$P < 0.0001$.

Fig. 3 PRMT1 interacts with YBX1 and regulates its phosphorylation in GSCs. (**A**) Venn diagram showing the overlap of PRMT1-interacting proteins identified by LC-MS/MS in GSC23, GSC11, and HEK293T cells. (**B**) Representative immunofluorescence images showing the colocalization of PRMT1 (red) and YBX1 (green) in the nuclei of GSC23 and GSC11 cells. Nuclei were counterstained with DAPI (blue). (**C**) Reciprocal Co-IP assays in GSC23 and GSC11 cells using anti-PRMT1 and anti-YBX1 antibodies, followed by immunoblotting with the indicated antibodies. IgG served as a negative control. (**D**) Co-IP analysis of exogenous PRMT1 and YBX1 in HEK293T cells co-transfected with FLAG-tagged PRMT1 and HA-tagged YBX1. Reciprocal immunoprecipitation was performed using anti-FLAG or anti-HA magnetic beads, followed by immunoblot analysis. (**E**, **F**) Integrated transcriptomic and

proteomic analyses showing changes in YBX1 expression after PRMT1 knockdown in GSC23 cells (**E**) or PRMT1 overexpression in GSC464 cells (**F**). (**G**) RT-qPCR analysis of YBX1 expression following PRMT1 knockdown in GSC23 and GSC11 cells, and following PRMT1 overexpression in GSC464 cells. (**H**) Western blotting analysis of PRMT1, total YBX1, and phospho-YBX1 (Ser102) in GSC23 and GSC11 cells following PRMT1 knockdown, and in GSC464 cells following overexpression of PRMT1. ***P < 0.001, ***P < 0.0001; n.s: not significant.

Fig. 4 PRMT1 activates AKT signaling to regulate YBX1 phosphorylation and nuclear translocation in GSCs. (**A**-**C**) Western blotting analysis of total AKT and phospho-AKT (Ser473) showing the effects of PRMT1 knockdown in GSC23 and GSC11 cells (**A**), pharmacological inhibition of PRMT1 with AMI-1 in GSC23 and GSC11 cells (**B**), and PRMT1 overexpression in GSC464 cells (**C**). (**D**-**F**) Western blotting analysis of total AKT, phospho-AKT (Ser473), total YBX1, and phospho-YBX1 (Ser102) showing the effects of AKT inhibition with MK2206 in GSC23 and GSC11 cells (**D**), and in GSC11 (**E**) and GSC23 (**F**) cells expressing control shRNA or shPRMT1, with or without MK2206 treatment. (**G**, **H**) Interaction between AKT and YBX1 was examined by exogenous Co-IP in HEK293T cells co-transfected with FLAG-tagged AKT and HA-tagged YBX1 (**G**) and by endogenous reciprocal Co-IP in GSC23 and GSC11 cells using anti-AKT and anti-YBX1 antibodies (**H**). IgG served as a negative control. (**I**, **J**) Representative immunofluorescence images showing YBX1 (red) localization in GSC23 cells following PRMT1 knockdown (**I**) and in HEK293T cells following PRMT1 overexpression (**J**). Nuclei were counterstained with DAPI (blue). Scale bars, 500 μm. (**K**, **L**) Immunoblotting analysis of YBX1 in cytoplasmic and nuclear fractions of GSC23 cells following PRMT1 knockdown (**K**) and of HEK293T cells following PRMT1 overexpression (**L**). GAPDH and Lamin B1 served as cytoplasmic and nuclear fraction controls, respectively. (**M**) Schematic diagram of PRMT1-mediated nuclear translocation of YBX1 in GSCs.

Fig. 5 PRMT1 methylates YBX1 at Arg69 in GSCs. (**A**) Schematic representation of the domain architecture of YBX1 protein and the cold-shock domain (CSD) deletion mutant. (**B**) Structural model of the PRMT1-YBX1 complex predicted by AlphaFold3,

identifying Arg69 (R69) within the YBX1 cold-shock domain as a putative methylation site at the interaction interface. (**C**) Mapping of the PRMT1-binding region in YBX1 by co-immunoprecipitation. HEK293T cells were co-transfected with FLAG-tagged PRMT1 and HA-tagged full-length or CSD-deletion YBX1 constructs. PRMT1 complexes were immunoprecipitated with anti-FLAG beads and analyzed by immunoblotting with an anti-HA antibody. (**D**, **E**) Endogenous YBX1 was immunoprecipitated from GSC23 and GSC11 cells following PRMT1 knockdown (**D**) or from GSC464 cells following PRMT1 overexpression (**E**), and YBX1-R69 methylation was detected by immunoblotting with an anti-YBX1-R69me2a antibody. (**F**) Endogenous YBX1 was immunoprecipitated from GSC23 cells treated with AMI-1 or AdOx, and asymmetric dimethylarginine (aDMA) and YBX1-R69 methylation levels were examined by immunoblotting with anti-aDMA and anti-YBX1-R69me2a antibodies. (**G**) HEK293T cells expressing HA-tagged YBX1 were treated with or without AdOx. YBX1 was immunoprecipitated with anti-HA beads, and aDMA and YBX1-R69 methylation were analyzed by immunoblotting. (**H**) GSC23 cells with stable PRMT1 knockdown were reconstituted with ectopic PRMT1 or vector control. Endogenous YBX1 was immunoprecipitated with an anti-YBX1 antibody, and aDMA and YBX1-R69 methylation levels were assessed by immunoblotting. (**I**) HEK293T cells were transfected with HA-tagged YBX1-WT or YBX1-R69K and treated with AMI-1. YBX1 was immunoprecipitated with anti-HA beads, and aDMA and YBX1-R69 methylation levels were examined by immunoblotting. (**J**) HEK293T cells were transfected with HA-tagged YBX1-WT or YBX1-R69K alone or together with FLAG-tagged PRMT1. YBX1 methylation was analyzed by immunoprecipitation with anti-HA beads followed by immunoblotting with an anti-YBX1-R69me2a antibody. (**K**) HEK293T cells expressing HA-tagged YBX1-WT or YBX1-R69K were subjected to YBX1 immunoprecipitation with anti-HA beads, followed by immunoblotting with anti-YBX1-R69me2a antibody in the absence or presence of the R69me2a peptide or the corresponding unmodified peptide.

Fig. 6 PRMT1-mediated YBX1 methylation at R69 is indispensable for GSC proliferation and self-renewal. (**A**) Reconstitution of YBX1-knockout GSC23 and

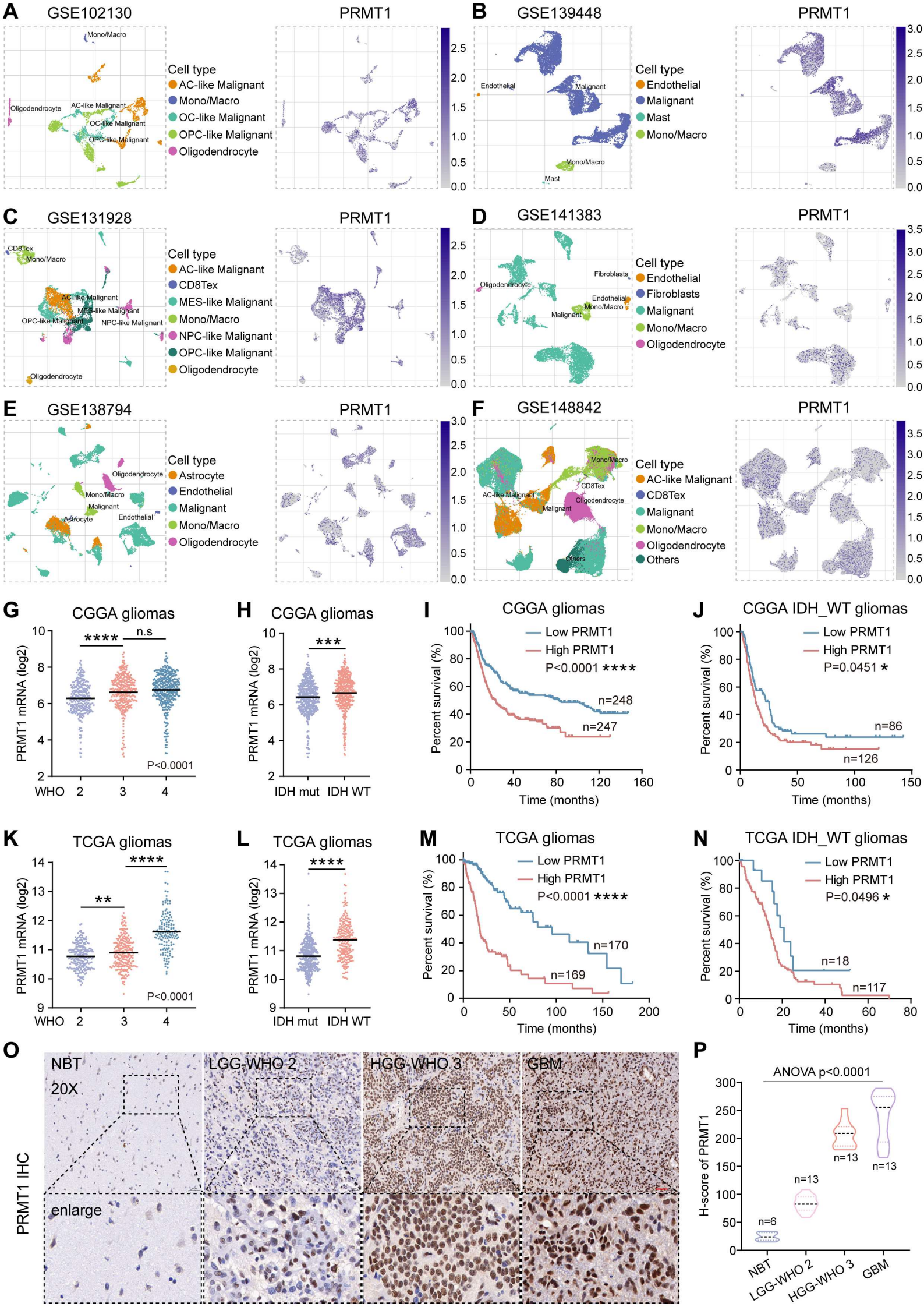
GSC11 cells with vector control, YBX1-WT, or the methylation-deficient mutant YBX1-R69K. Immunoblot analysis confirmed YBX1 re-expression and loss of YBX1-R69me2a in the R69K mutant. (**B**) CCK-8 assays show proliferation of reconstituted GSC23 cells. (**C**) ELDA of sphere-forming frequency in reconstituted GSC23 cells. (**D-H**) Orthotopic intracranial xenograft assays using reconstituted GSC23 cells expressing vector control, YBX1-WT, or YBX1-R69K. Representative H&E staining of whole-brain sections and immunohistochemical staining for Ki67 and YBX1-R69me2a in xenograft tumors (**D**). Quantification of tumor area (**E**). Kaplan-Meier survival analysis of tumor-bearing mice (**F**). H-score quantification of Ki67 (**G**) and YBX1-R69me2a (**H**) staining. Scale bars, 5 mm for H&E images and 50 μm for IHC staining. (**I-N**) Competitive inhibition of YBX1 methylation by synthetic peptides. Schematic representation of the amino acid sequences of the TAT-fused non-methylated peptide and the corresponding TAT-fused methylated peptide (**I**). GSC23 and GSC11 cells were treated with peptides (20 μM, 48 h), followed by YBX1 immunoprecipitation and immunoblot analysis of YBX1-R69 methylation using a site-specific anti-YBX1-R69me2a antibody (**J**). HEK293T cells co-transfected with FLAG-tagged PRMT1 and HA-tagged YBX1 were treated with methylated or non-methylated YBX1 peptides (20 μM, 48 h), followed by immunoprecipitation with anti-FLAG beads and immunoblot analysis (**K**). CCK-8 assays of GSC23 (**L**) and GSC11 (**M**) cells treated with methylated or non-methylated YBX1 peptides for 48 h. ELDA of sphere-forming frequency in GSC23 and GSC11 cells treated with methylated or non-methylated YBX1 peptides (20 μM) (**N**). (**O-R**) *In vivo* antitumor effects of peptide-mediated inhibition of YBX1 methylation. Nude mice bearing established subcutaneous GSC23 xenografts were randomized to receive peptides (10 mg/kg, intraperitoneally, every other day for 2 weeks). Representative images of tumors collected at the endpoint are shown in (**O**). Representative H&E staining and Ki67 immunohistochemistry of tumor sections are shown in (**P**). Tumor growth curves are shown in (**Q**), and H-score quantification of Ki67 staining is shown in (**R**). Scale bar, 10 μm. **P < 0.01, ***P < 0.001, ****P < 0.0001; n.s: not significant.

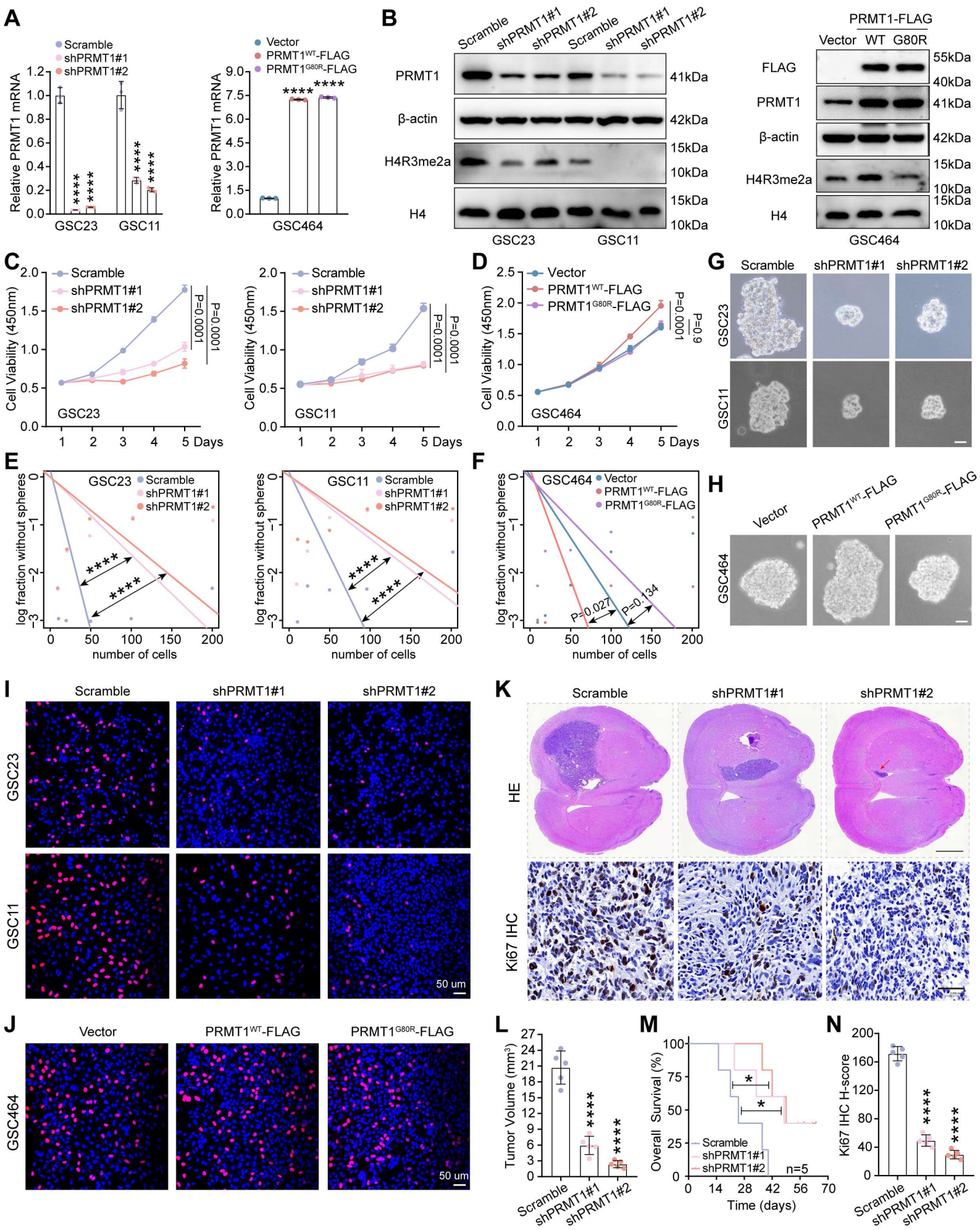
Fig. 7 The PRMT1-YBX1 axis stabilizes *PKMYT1* and *CDCA5* transcripts in GSCs.

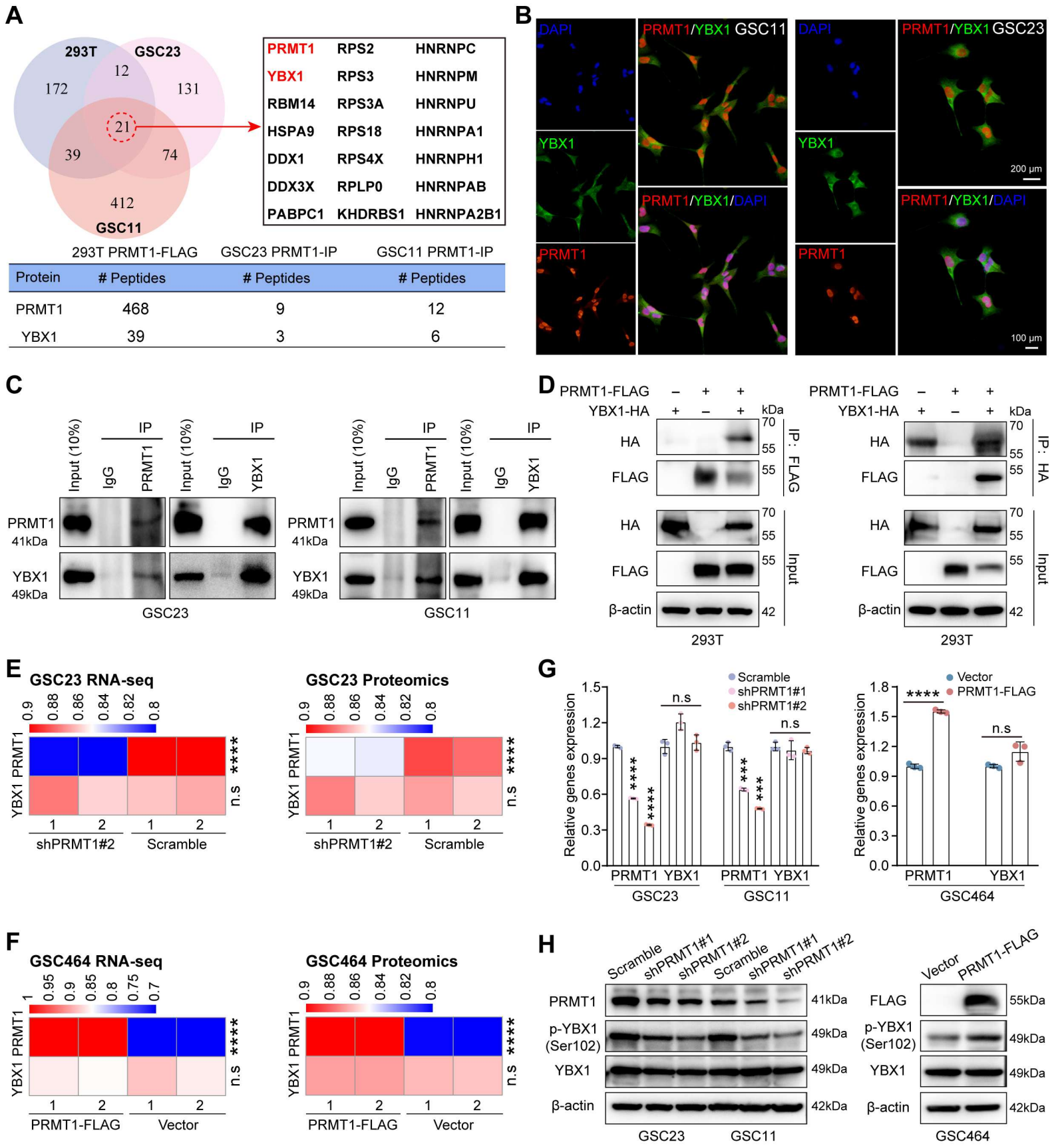
(**A**) Venn diagram showing the overlap among genes downregulated following PRMT1 knockdown in GSC23 cells, genes downregulated following YBX1 knockdown in U251 cells, and YBX1-bound transcripts identified by eCLIP-seq in U251 cells. (**B**) De novo motif analysis of the top 2,000 YBX1 eCLIP-seq peaks using HOMER (v4.11.2), showing the top-ranked 4-bp motif. (**C**) IGV tracks of YBX1 eCLIP-seq and input control signals across the PKMYT1 and CDCA5 loci. (**D-G**) PRMT1 regulates PKMYT1 and CDCA5 expressions. RT-qPCR analysis of *PKMYT1* and *CDCA5* mRNA levels in GSC23 and GSC11 cells following PRMT1 knockdown (**D**) and in GSC464 cells following PRMT1 overexpression (**E**). Immunoblot analysis of PKMYT1 and CDCA5 protein levels in GSC23 and GSC11 cells following PRMT1 knockdown (**F**) and in GSC464 cells following PRMT1 overexpression (**G**). H-K) YBX1 regulates PKMYT1 and CDCA5 expressions. RT-qPCR analysis of *PKMYT1* and *CDCA5* mRNA levels in GSC23 and GSC11 cells following YBX1 knockdown (**H**) and in GSC464 cells following YBX1 overexpression (**I**). Immunoblot analysis of PKMYT1 and CDCA5 protein levels in GSC23 and GSC11 cells following YBX1 knockdown (**J**) and in GSC464 cells following YBX1 overexpression (**K**). (**L-O**) PRMT1 promotes YBX1 binding to *PKMYT1* and *CDCA5* transcripts. RIP-qPCR assays using an anti-YBX1 antibody validated the association of YBX1 with *CDCA5* (**L**) and *PKMYT1* (**M**) mRNAs in GSC23 and GSC11 cells; IgG served as a negative control. RIP-qPCR analysis further showed the effects of PRMT1 knockdown on YBX1 binding to *CDCA5* (**N**) and *PKMYT1* (**O**) transcripts in GSC23 and GSC11 cells. (**P-S**) PRMT1 and YBX1 regulate the stability of *PKMYT1* and *CDCA5* mRNAs. Cells were treated with actinomycin D for the indicated times (0, 2, 4, 6, and 8 h), and mRNA decay was measured by RT-qPCR in GSC23 cells following PRMT1 knockdown for CDCA5 (**P**) and PKMYT1 (**Q**), or following YBX1 knockdown for CDCA5 (**R**) and PKMYT1 (**S**). *P < 0.05, **P < 0.01, ***P < 0.001, ****P < 0.0001.

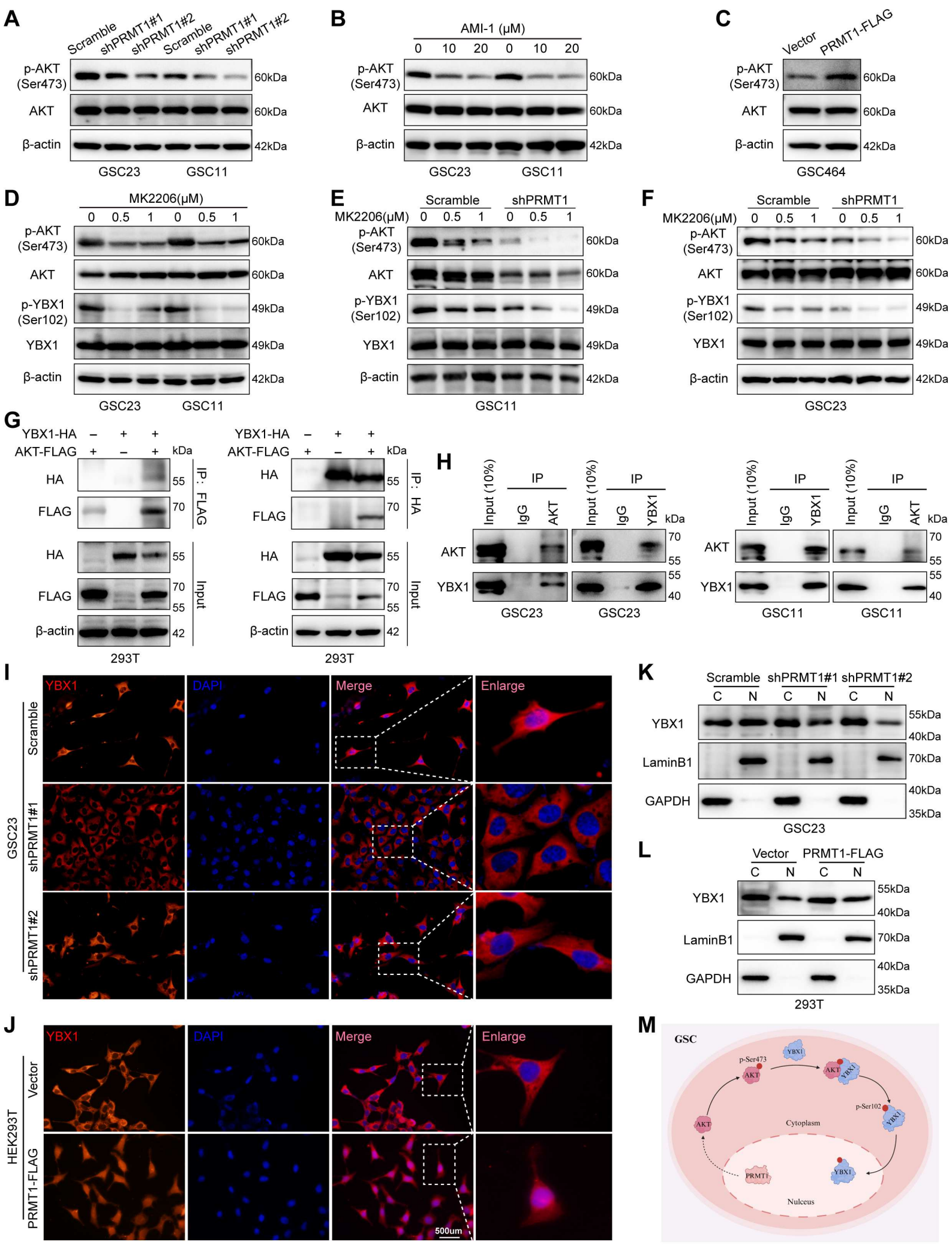
Fig. 8 Clinical relevance of the PRMT1-YBX1 signaling axis in glioma. (**A**, **B**) Representative immunohistochemical images of YBX1-R69me2a in non-tumor brain tissues, lower-grade glioma (LGG, WHO grade 2), high-grade glioma (HGG, WHO grade 3), and GBM specimens (**A**), and quantification of YBX1-R69me2a staining

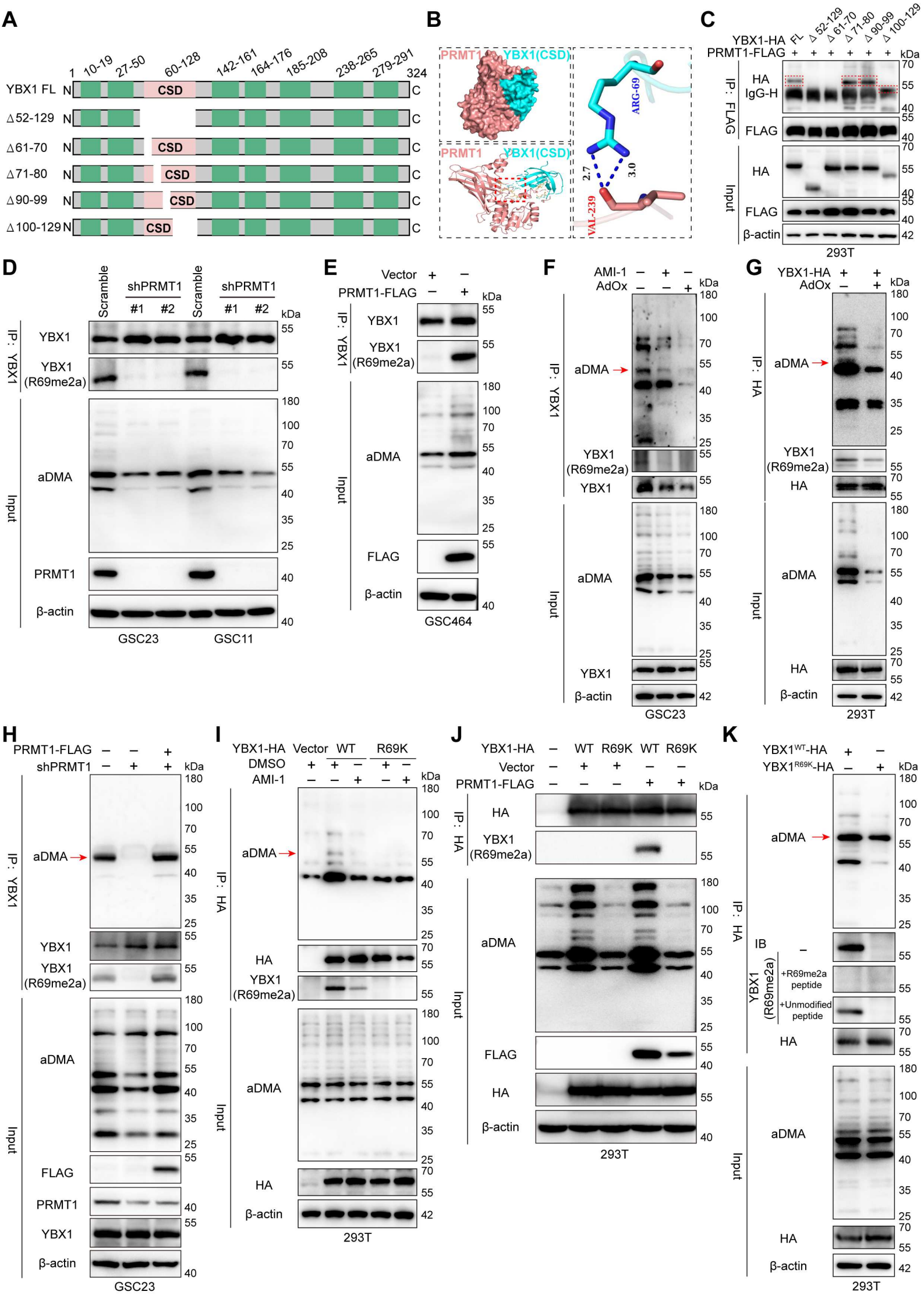
intensity (**B**). Scale bar, 100 μm. (**C**) Pearson correlation analysis between PRMT1 and YBX1-R69me2a immunohistochemical scores across 39 glioma specimens. (**D**-**G**) Immunoblotting analysis of PRMT1, YBX1-R69me2a, NSUN2, CDCA5, and PKMYT1 expression in glioma tissues (n = 39) and NBTs (n = 6) (**D**). Correlation analyses based on immunoblot quantification showing the associations between PRMT1 and YBX1-R69me2a (**E**), PRMT1 and CDCA5 (**F**), and PRMT1 and PKMYT1 (**G**) in glioma samples. (**H**, **I**) Kaplan-Meier analysis of overall survival in glioma patients stratified by PRMT1 (**H**) or YBX1-R69me2a (**I**) immunohistochemical staining intensity. Data are presented as mean ± SD. Pearson correlation analysis was used in (**C**) and (**E**-**G**), and survival differences were assessed by the log-rank test in (**H**, **I**). (**J**) Schematic diagram of PRMT1-YBX1-CDCA5/PKMYT1 axis-mediated GSC proliferation and self-renewal.

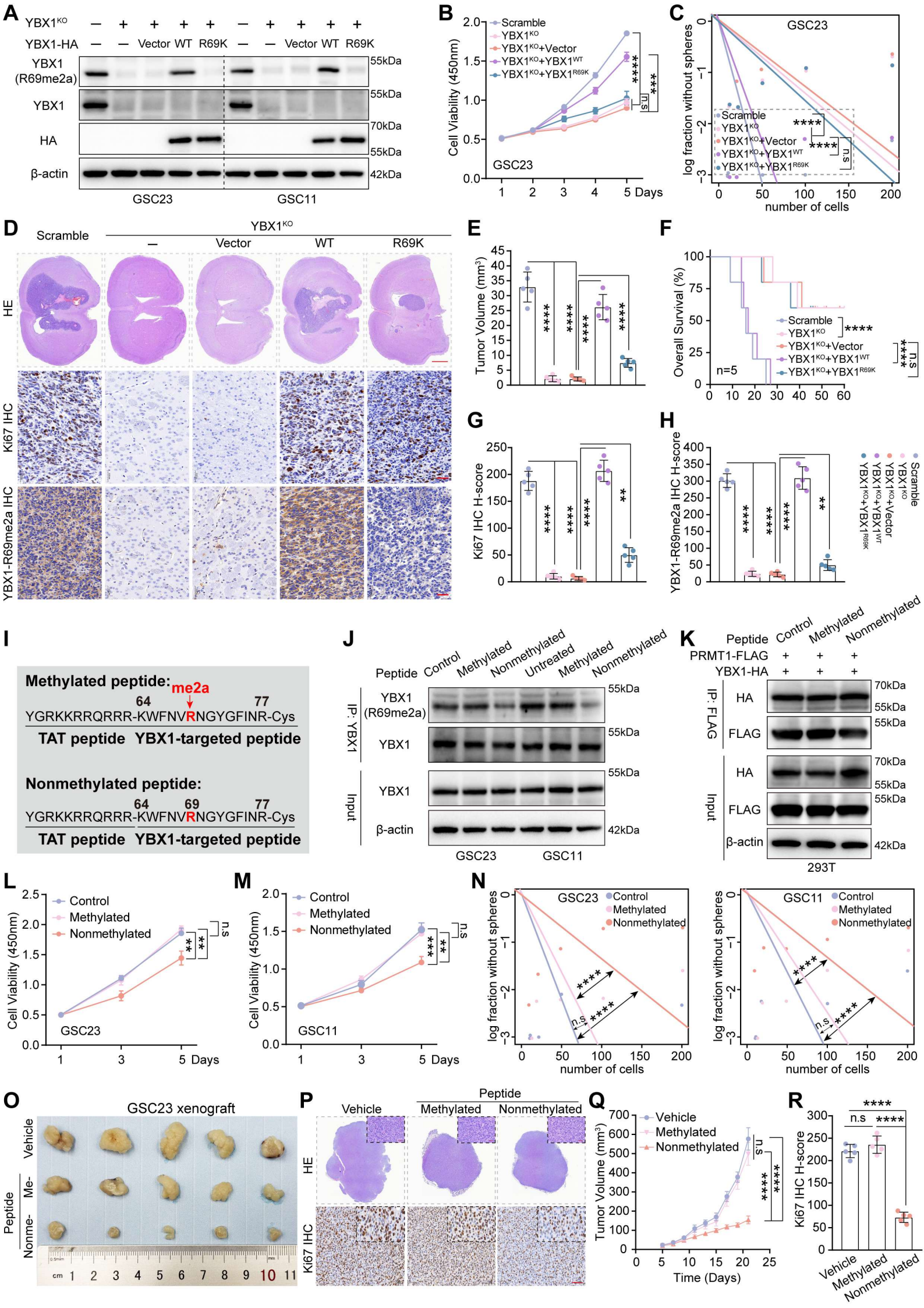

A
GSE102130
PRMT1
Mono/Macro
Oligodendrocyte
AC-like Malignant
OC-like Malignant
OPC-like Malignant
Cell type
AC-like Malignant
Mono/Macro
OC-like Malignant
OPC-like Malignant
Oligodendrocyte
B
GSE139448
PRMT1
Endothelial
Malignant
Mono/Macro
Mast
Cell type
Endothelial
Malignant
Mast
Mono/Macro
C
GSE131928
PRMT1
CD8Tex
Mono/Macro
AC-like Malignant
MES-like Malignant
OPC-like Malignant
NPC-like Malignant
Oligodendrocyte
Cell type
AC-like Malignant
CD8Tex
MES-like Malignant
Mono/Macro
NPC-like Malignant
OPC-like Malignant
Oligodendrocyte
D
GSE141383
PRMT1
Fibroblasts
Oligodendrocyte
Endothelial
Mono/Macro
Malignant
Cell type
Endothelial
Fibroblasts
Malignant
Mono/Macro
Oligodendrocyte
E
GSE138794
PRMT1
Oligodendrocyte
Mono/Macro
Malignant
Astrocyte
Endothelial
Cell type
Astrocyte
Endothelial
Malignant
Mono/Macro
Oligodendrocyte
F
GSE148842
PRMT1
Mono/Macro
CD8Tex
AC-like Malignant
Oligodendrocyte
Malignant
Others
Cell type
AC-like Malignant
CD8Tex
Malignant
Mono/Macro
Oligodendrocyte
Others
G
CGGA gliomas
PRMT1 mRNA (log2)
****
n.s
P<0.0001
WHO 2 3 4
H
CGGA gliomas
PRMT1 mRNA (log2)
***
IDH mut IDH WT
I
CGGA gliomas
Low PRMT1
High PRMT1
P<0.0001 ****
n=248
n=247
Percent survival (%)
Time (months)
J
CGGA IDH_WT gliomas
Low PRMT1
High PRMT1
P=0.0451 *
n=86
n=126
Percent survival (%)
Time (months)
K
TCGA gliomas
PRMT1 mRNA (log2)
**
****
P<0.0001
WHO 2 3 4
L
TCGA gliomas
PRMT1 mRNA (log2)
****
IDH mut IDH WT
M
TCGA gliomas
Low PRMT1
High PRMT1
P<0.0001 ****
n=170
n=169
Percent survival (%)
Time (months)
N
TCGA IDH_WT gliomas
Low PRMT1
High PRMT1
P=0.0496 *
n=18
n=117
Percent survival (%)
Time (months)
O
PRMT1 IHC
NBT
20X
LGG-WHO 2
HGG-WHO 3
GBM
enlarge
P
ANOVA p<0.0001
H-score of PRMT1
n=6
n=13
n=13
n=13
NBT
LGG-WHO 2
HGG-WHO 3
GBM

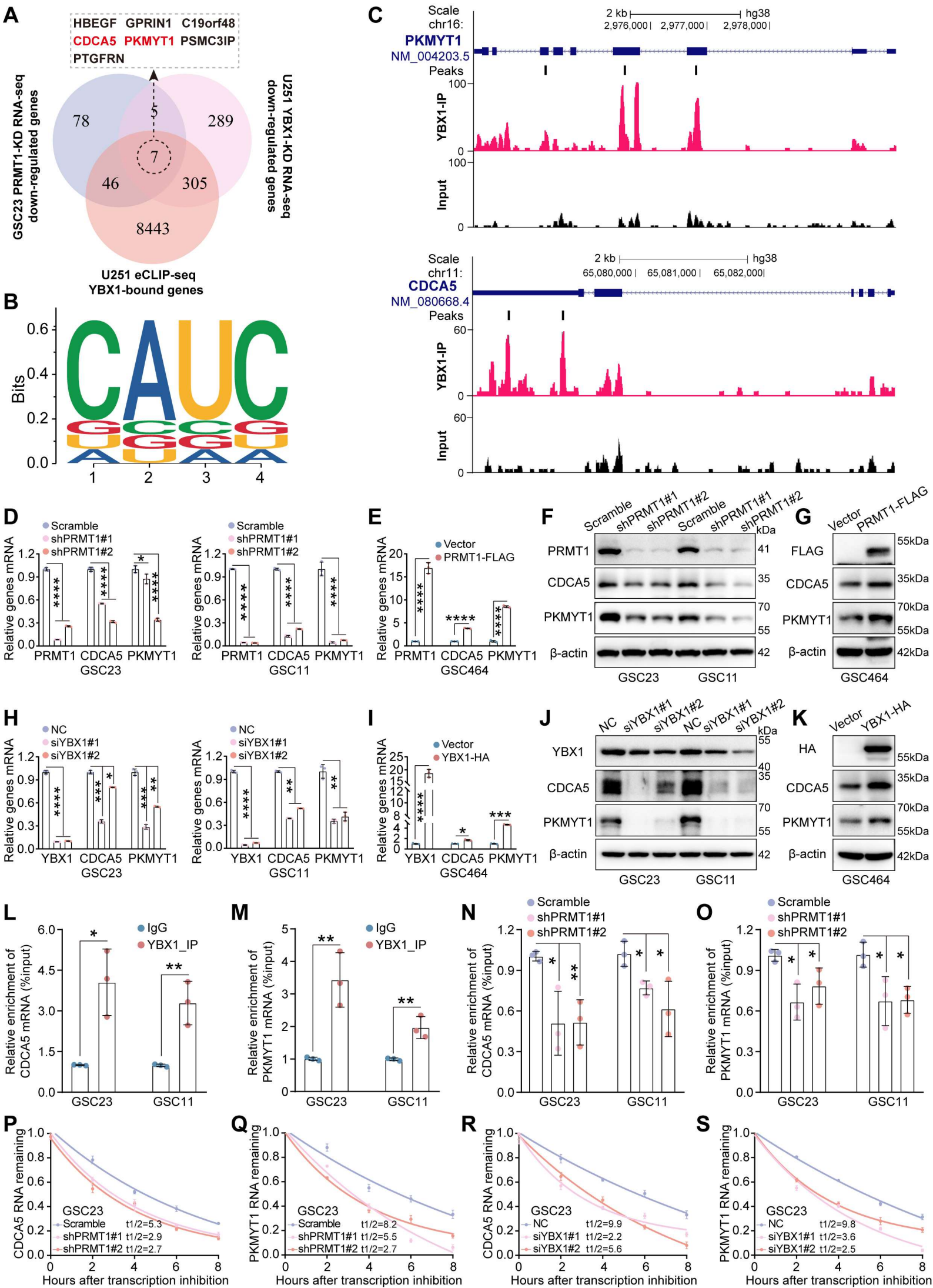

A
Scramble
shPRMT1#1
shPRMT1#2
Relative PRMT1 mRNA
GSC23
GSC11
Vector
PRMT1WT-FLAG
PRMT1G80R-FLAG
GSC464
B
Scramble
shPRMT1#1
shPRMT1#2
PRMT1
β-actin
H4R3me2a
H4
41kDa
42kDa
15kDa
10kDa
PRMT1-FLAG
Vector
WT
G80R
FLAG
55kDa
40kDa
C
Cell Viability (450nm)
Days
P=0.0001
D
P=0.9
G
H
E
F
log fraction without spheres
number of cells
P=0.027
P=0.134
I
50 um
J
K
HE
Ki67 IHC
L
Tumor Volume (mm3)
M
Overall Survival (%)
n=5
N
Ki67 IHC H-score

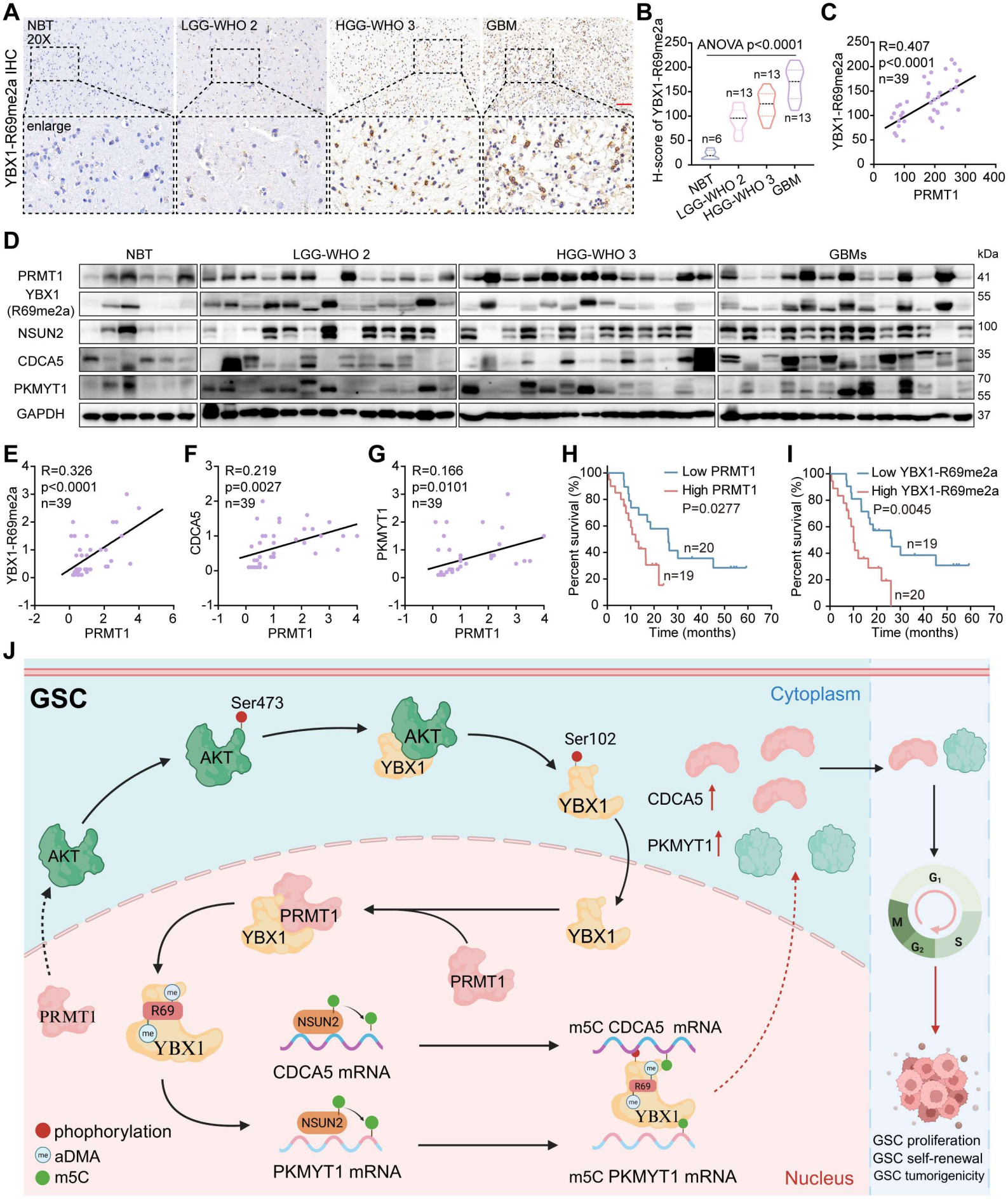

A
293T
GSC23
GSC11
172
12
131
21
39
74
412
PRMT1 RPS2 HNRNPC
YBX1 RPS3 HNRNPM
RBM14 RPS3A HNRNPU
HSPA9 RPS18 HNRNPA1
DDX1 RPS4X HNRNPH1
DDX3X RPLP0 HNRNPAB
PABPC1 KHDRBS1 HNRNPA2B1
293T PRMT1-FLAG
GSC23 PRMT1-IP
GSC11 PRMT1-IP
Protein # Peptides # Peptides # Peptides
PRMT1 468 9 12
YBX1 39 3 6
B
DAPI
PRMT1/YBX1 GSC11
YBX1
PRMT1
PRMT1/YBX1/DAPI
PRMT1/YBX1 GSC23
200 μm
100 μm
C
Input (10%)
IP
IgG
PRMT1
YBX1
PRMT1 41kDa
YBX1 49kDa
GSC23
GSC11
D
PRMT1-FLAG
YBX1-HA
kDa
HA
FLAG
β-actin
IP: FLAG
IP: HA
Input
293T
E
GSC23 RNA-seq
GSC23 Proteomics
shPRMT1#2
Scramble
n.s
****
F
GSC464 RNA-seq
GSC464 Proteomics
PRMT1-FLAG
Vector
G
Scramble
shPRMT1#1
shPRMT1#2
Relative genes expression
PRMT1 YBX1
GSC23
GSC11
Vector
PRMT1-FLAG
GSC464
H
Scramble
shPRMT1#1
shPRMT1#2
PRMT1
p-YBX1 (Ser102)
YBX1
β-actin
FLAG
Vector
PRMT1-FLAG


A
Scramble
shPRMT1#1
shPRMT1#2
Scramble
shPRMT1#1
shPRMT1#2
p-AKT (Ser473)
AKT
β-actin
60kDa
60kDa
42kDa
GSC23
GSC11
B
AMI-1 (μM)
0 10 20 0 10 20
p-AKT (Ser473)
AKT
β-actin
60kDa
60kDa
42kDa
GSC23
GSC11
C
Vector
PRMT1-FLAG
p-AKT (Ser473)
AKT
β-actin
60kDa
60kDa
42kDa
GSC464
D
MK2206(μM)
0 0.5 1 0 0.5 1
p-AKT (Ser473)
AKT
p-YBX1 (Ser102)
YBX1
β-actin
60kDa
60kDa
49kDa
49kDa
42kDa
GSC23
GSC11
E
Scramble
shPRMT1
MK2206(μM) 0 0.5 1 0 0.5 1
p-AKT (Ser473)
AKT
p-YBX1 (Ser102)
YBX1
β-actin
60kDa
60kDa
49kDa
49kDa
42kDa
GSC11
F
Scramble
shPRMT1
MK2206(μM) 0 0.5 1 0 0.5 1
p-AKT (Ser473)
AKT
p-YBX1 (Ser102)
YBX1
β-actin
60kDa
60kDa
49kDa
49kDa
42kDa
GSC23
G
YBX1-HA – + +
AKT-FLAG + – +
kDa
HA
FLAG
IP : FLAG
55
70
HA
FLAG
β-actin
Input
55
70 55
42
293T
YBX1-HA – + +
AKT-FLAG + – +
kDa
HA
FLAG
IP : HA
55
70
HA
FLAG
β-actin
Input
55
70 55
42
293T
H
Input (10%)
IP
IgG
AKT
YBX1
kDa
AKT
YBX1
70
55
55
40
GSC23
GSC23
GSC11
GSC11
I
YBX1
DAPI
Merge
Enlarge
Scramble
shPRMT1#1
shPRMT1#2
GSC23
J
YBX1
DAPI
Merge
Enlarge
Vector
PRMT1-FLAG
HEK293T
500um
K
Scramble
shPRMT1#1
shPRMT1#2
C N C N C N
YBX1
LaminB1
GAPDH
55kDa
40kDa
70kDa
40kDa
35kDa
GSC23
L
Vector
PRMT1-FLAG
C N C N
YBX1
LaminB1
GAPDH
55kDa
40kDa
70kDa
40kDa
35kDa
293T
M
GSC
p-Ser473
AKT
YBX1
AKT
YBX1
p-Ser102
YBX1
AKT
Cytoplasm
PRMT1
YBX1
Nulceus


A
1 10-19 27-50 60-128 142-161 164-176 185-208 238-265 279-291 324
YBX1 FL N CSD C
Δ52-129 N C
Δ61-70 N CSD C
Δ71-80 N CSD C
Δ90-99 N CSD C
Δ100-129 N CSD C
B
PRMT1 YBX1(CSD)
PRMT1 YBX1(CSD)
ARG-69
VAL-239
2.7
3.0
C
YBX1-HA FL Δ52-129 Δ61-70 Δ71-80 Δ90-99 Δ100-129
PRMT1-FLAG + + + + + +
kDa
IP: FLAG
HA
IgG-H
FLAG
Input
HA
FLAG
β-actin
293T
D
Scramble shPRMT1 #1 #2 Scramble shPRMT1 #1 #2
kDa
IP: YBX1
YBX1
YBX1 (R69me2a)
Input
aDMA
PRMT1
β-actin
GSC23 GSC11
E
Vector + –
PRMT1-FLAG – +
kDa
IP: YBX1
YBX1
YBX1 (R69me2a)
Input
aDMA
FLAG
β-actin
GSC464
F
AMI-1 – + –
AdOx – – +
kDa
IP: YBX1
aDMA
YBX1 (R69me2a)
YBX1
Input
aDMA
YBX1
β-actin
GSC23
G
YBX1-HA + +
AdOx – +
kDa
IP: HA
aDMA
YBX1 (R69me2a)
HA
Input
aDMA
HA
β-actin
293T
H
PRMT1-FLAG – – +
shPRMT1 – + +
kDa
IP: YBX1
aDMA
YBX1
YBX1 (R69me2a)
Input
aDMA
FLAG
PRMT1
YBX1
β-actin
GSC23
I
YBX1-HA Vector WT R69K
DMSO + + – + –
AMI-1 – – + – +
kDa
IP: HA
aDMA
HA
YBX1 (R69me2a)
Input
aDMA
HA
β-actin
293T
J
YBX1-HA – WT R69K WT R69K
Vector – + + – –
PRMT1-FLAG – – – + +
kDa
IP: HA
HA
YBX1 (R69me2a)
Input
aDMA
FLAG
HA
β-actin
293T
K
YBX1WT-HA + –
YBX1R69K-HA – +
kDa
IP: HA
aDMA
IB
YBX1 (R69me2a)
–
+R69me2a peptide
+Unmodified peptide
HA
Input
aDMA
HA
β-actin
293T


A
YBX1KO
YBX1-HA
Vector WT R69K Vector WT R69K
YBX1 (R69me2a)
YBX1
HA
β-actin
55kDa
70kDa
42kDa
GSC23
GSC11
B
Scramble
YBX1KO
YBX1KO+Vector
YBX1KO+YBX1WT
YBX1KO+YBX1R69K
Cell Viability (450nm)
GSC23
Days
C
GSC23
log fraction without spheres
number of cells
D
Scramble
YBX1KO
Vector WT R69K
HE
Ki67 IHC
YBX1-R69me2a IHC
E
Tumor Volume (mm3)
F
Overall Survival (%)
n=5
G
Ki67 IHC H-score
H
YBX1-R69me2a IHC H-score
I
Methylated peptide:
me2a
64 77
YGRKKRRQRRR-KWFNVRNGYGFINR-Cys
TAT peptide YBX1-targeted peptide
Nonmethylated peptide:
64 69 77
YGRKKRRQRRR-KWFNVRNGYGFINR-Cys
TAT peptide YBX1-targeted peptide
J
Peptide Control Methylated Nonmethylated Untreated Methylated Nonmethylated
IP: YBX1
Input
YBX1 (R69me2a)
YBX1
β-actin
GSC23 GSC11
K
Peptide Control Methylated Nonmethylated
PRMT1-FLAG
YBX1-HA
IP: FLAG
Input
HA
FLAG
β-actin
293T
L
Control
Methylated
Nonmethylated
Cell Viability (450nm)
GSC23
Days
M
GSC11
N
GSC23
GSC11
log fraction without spheres
number of cells
O
GSC23 xenograft
Vehicle
Peptide
Me-
Nonme-
P
Vehicle
Peptide
Methylated Nonmethylated
HE
Ki67 IHC
Q
Tumor Volume (mm3)
Time (Days)
R
Ki67 IHC H-score
Vehicle
Methylated
Nonmethylated


A
HBEGF GPRIN1 C19orf48
CDCA5 PKMYT1 PSMC3IP
PTGFRN
GSC23 PRMT1-KD RNA-seq down-regulated genes
U251 YBX1-KD RNA-seq down-regulated genes
U251 eCLIP-seq YBX1-bound genes
78
5
289
7
46
305
8443
B
Bits
C
Scale
chr16:
2 kb
hg38
2,976,000
2,977,000
2,978,000
PKMYT1
NM_004203.5
Peaks
YBX1-IP
Input
chr11:
65,080,000
65,081,000
65,082,000
CDCA5
NM_080668.4
D
Scramble
shPRMT1#1
shPRMT1#2
Relative genes mRNA
PRMT1 CDCA5 PKMYT1
GSC23
GSC11
E
Vector
PRMT1-FLAG
GSC464
F
PRMT1
CDCA5
PKMYT1
β-actin
kDa
G
FLAG
H
NC
siYBX1#1
siYBX1#2
YBX1
I
YBX1-HA
J
K
L
IgG
YBX1_IP
Relative enrichment of CDCA5 mRNA (%input)
M
Relative enrichment of PKMYT1 mRNA (%input)
N
O
P
CDCA5 RNA remaining
Hours after transcription inhibition
GSC23
Scramble t1/2=5.3
shPRMT1#1 t1/2=2.9
shPRMT1#2 t1/2=2.7
Q
PKMYT1 RNA remaining
Scramble t1/2=8.2
shPRMT1#1 t1/2=5.5
shPRMT1#2 t1/2=2.7
R
NC t1/2=9.9
siYBX1#1 t1/2=2.2
siYBX1#2 t1/2=5.6
S
NC t1/2=9.8
siYBX1#1 t1/2=3.6
siYBX1#2 t1/2=2.5


A
NBT
20X
LGG-WHO 2
HGG-WHO 3
GBM
enlarge
YBX1-R69me2a IHC
B
ANOVA p<0.0001
H-score of YBX1-R69me2a
n=6
n=13
n=13
n=13
NBT
LGG-WHO 2
HGG-WHO 3
GBM
C
R=0.407
p<0.0001
n=39
YBX1-R69me2a
PRMT1
D
NBT
LGG-WHO 2
HGG-WHO 3
GBMs
kDa
PRMT1
YBX1 (R69me2a)
NSUN2
CDCA5
PKMYT1
GAPDH
41
55
100
35
70
55
37
E
R=0.326
p<0.0001
n=39
YBX1-R69me2a
PRMT1
F
R=0.219
p=0.0027
n=39
CDCA5
PRMT1
G
R=0.166
p=0.0101
n=39
PKMYT1
PRMT1
H
Low PRMT1
High PRMT1
P=0.0277
n=20
n=19
Percent survival (%)
Time (months)
I
Low YBX1-R69me2a
High YBX1-R69me2a
P=0.0045
n=19
n=20
Percent survival (%)
Time (months)
J
GSC
Cytoplasm
Ser473
AKT
AKT
YBX1
Ser102
YBX1
CDCA5
PKMYT1
AKT
PRMT1
YBX1
YBX1
PRMT1
PRMT1
me
R69
me
YBX1
NSUN2
CDCA5 mRNA
m5C CDCA5 mRNA
me
R69
me
YBX1
NSUN2
PKMYT1 mRNA
m5C PKMYT1 mRNA
phophorylation
me aDMA
m5C
Nucleus
G1
S
G2
M
GSC proliferation
GSC self-renewal
GSC tumorigenicity

Supplementary Files

This is a list of supplementary files associated with this preprint. Click to download.

- Supplementarymaterials.docx